Behaviour of Sr, Ca, and Mg isotopes under variable hydrological conditions in high-relief large river systems

Bei-Bei Chen [a, b], Si-Liang Li [b, c *], Philip A.E. Pogge von Strandmann [d, e], David J. Wilson [d], Jun Zhong [b], Ting-Ting Ma [b], Jian Sun [f], Cong-Qiang Liu [b]

a State Key Laboratory of Geological Processes and Mineral Resources, China University of Geosciences, Beijing

b Institute of Surface-Earth System Science, School of Earth System Science, Tianjin University, Tianjin 300072, China

c State Key Laboratory of Hydraulic Engineering Simulation and Safety, Tianjin University, Tianjin 300072, China

d London Geochemistry and Isotope Centre (LOGIC), Institute of Earth and Planetary Sciences, University College London and Birkbeck, University of London, Gower Street, London WC1E 6BT, UK

e Mainz Isotopes and Geochemistry (MIGHTY), Institute of Geosciences, Johannes Gutenberg University, 55122 Mainz, Germany

f Key Laboratory of Deep-Earth Dynamics of Ministry of Natural Resources, MNR Key Laboratory of Isotope Geology, Institute of Geology, Chinese Academy of Geological Sciences, Beijing 100037, China

Manuscript submitted to *Geochimica et Cosmochimica Acta* (07-09-2022)

*Corresponding author: Si-Liang Li

Email: Siliang.li@tju.edu.cn

Abstract

To assess how chemical weathering processes in large high-relief river systems respond to climatic variability, we studied seasonal changes in radiogenic strontium ($^{87}Sr/^{86}Sr$) and stable calcium ($\delta^{44/40}Ca$) and magnesium ($\delta^{26}Mg$) isotopes in the Jinsha and Yalong rivers, which drain the southeastern Tibetan Plateau. During the low-runoff season, with discharge (Q) <2000 m^3/s, the river waters reflect the Sr, Ca, and Mg isotope signatures of recharge meltwaters, with additional isotope fractionation signals for Ca and Mg related to secondary mineral precipitation, which might imply that meltwater flushes soil solutions from the soil. During medium-runoff intervals ($2000m^3/s<Q<4000m^3/s$), the Sr, Ca, and Mg isotope signatures in the Jinsha river waters are similar to those of the headwaters, which are influenced by evaporite dissolution, while the Yalong is affected by greater carbonate weathering relative to silicate weathering. In both rivers, bedrock dissolution governs the chemical composition of the river waters. During the high-runoff season ($Q>4000m^3/s$), storms generate rapid overland flow, which transfers large volumes of soil into the rivers, such that soil weathering plays an important role in regulating riverine chemical compositions. At these times, the riverine Ca and Sr isotope evolution is influenced by secondary mineral dissolution and sediment-water cation exchange. Overall, this study highlights the potential of combining multiple isotope systems (Sr, Ca, Mg) to trace the dynamics of water-rock interaction under variable hydrological conditions.

Keywords: Chemical weathering; Hydrological condition; Water-rock interaction; Ca

isotopes; Mg isotopes; Tibetan Plateau.

1 Introduction

During silicate rock weathering, primary minerals are dissolved by carbonic acid, releasing ions and alkalinity into river waters. Following their transport to the ocean, calcium (Ca) and magnesium (Mg) are ultimately precipitated from seawater as carbonates, which impacts long-term global climate (Berner and Berner, 2012). However, the sensitivity of chemical weathering in response to climatic factors (e.g. runoff, temperature) remains controversial (Deng et al., 2022; Maher and Chamberlain, 2014; Riebe et al., 2004; West et al., 2005).

Large river systems homogenize chemical characteristics from different processes, which provides an opportunity to address the major controls on chemical weathering at a continental scale (Stallard and Edmond, 1983; Tipper et al., 2012c). Furthermore, evaluating river water chemistry in the context of temporal variations in hydrological processes offers a unique chance to determine the response of chemical weathering to climatic changes. For example, seasonal variations in water-rock interaction time (Rai and Singh, 2007; Tipper et al., 2006c; Tripathy et al., 2010), changes in the dominant fluid flow path (Calmels et al., 2011; Torres et al., 2015), solute supply from different lithological units (Bickle et al., 2003; Boral et al., 2021; Chao et al., 2015), or input from additional sources (e.g. plant litter, dust, mine water) (Hindshaw et al., 2019; Pett-Ridge et al., 2009; Zieliński et al., 2018) may all contribute to temporal variations in river water chemistry within a single catchment. In addition to these hydrologic

processes impacting the inputs, secondary processes such as cation exchange (Tipper et al., 2021), adsorption by clay minerals (Michalopoulos and Aller, 1995), secondary mineral neoformation (carbonates, silicates, and oxides) (Jacobson et al., 2002), plant growth (Berner, 1997) can also vary in response to changing hydrological conditions (Clow and Mast, 2010; Maher, 2011), but they can be hard to identify based on only the dissolved concentrations of major and trace elements (Pett-Ridge et al., 2009). As such, the impact of secondary processes on the chemical composition of river water under different hydrological conditions is currently unclear, and the lack of relevant studies hinders our understanding of the chemical weathering process.

Fortunately, the development of metal stable isotope measurements has provided a new perspective for understanding chemical weathering processes (Sullivan et al., 2016). In particular, stable Ca and Mg isotopes have attracted attention because Ca and Mg are major elements in many Earth surface reservoirs (e.g. rocks, waters, plants), represent important nutrients in the ecosystem (Griffith et al., 2020; Tipper, 2022), and their elemental cycles are directly coupled to the carbon cycle through silicate weathering and carbonate precipitation (Berner and Berner, 2012; Wimpenny et al., 2011). Stable Ca and Mg isotopes can be fractionated during the secondary processes described above and can therefore be used to trace these processes within weathering environments (Cenki-Tok et al., 2009; Ewing et al., 2008; Fan et al., 2016; Fantle and Tipper, 2014; Fries et al., 2019; Holmden and Bélanger, 2010; Ma et al., 2015; Nelson et al., 2021; Nelson et al., 2022; Opfergelt et al., 2014; Ryu et al., 2016; Saulnier et al., 2012; Tipper et al., 2006a; Tipper et al., 2012a; Wimpenny et al., 2014; Wimpenny et

al., 2010). Although rock endmembers have a wide range of Ca and Mg isotopic compositions, which represents a challenge for distinguishing the controls (solute sources vs. secondary fractionation) on riverine Ca and Mg isotopes (Fantle and Tipper, 2014; Pogge von Strandmann et al., 2019b; Tipper et al., 2006a; Tipper et al., 2008), radiogenic strontium (Sr) isotopes can provide complementary evidence to deconvolve fractionation and lithological controls (Tipper et al., 2006c). By conducting a multi-isotope study (stable Ca and Mg, and radiogenic Sr), the significance of secondary processes can be constrained, thereby enabling a better assessment of the controls on chemical weathering.

Previous studies have suggested that seasonal variations in riverine Ca and Mg isotopes are related to catchment size (Griffith et al., 2020; Tipper, 2022). In small catchments, temporal variations of Ca and Mg isotopes respond to both vegetation and water-rock interactions (Cenki-Tok et al., 2009; Dessert et al., 2015; Lehn et al., 2017; Tipper et al., 2008; Tipper et al., 2012b), leading to the potential to use these isotope systems to explore the inter-relationships between plants and chemical weathering (Bolou-Bi et al., 2012; Cenki-Tok et al., 2009). In contrast, the factors controlling temporal variations in Ca and Mg isotopes in large river systems remain poorly constrained, with only a few studies having been conducted on large rivers over seasonal timescales (Hindshaw et al., 2019; Mavromatis et al., 2020; Négrel et al., 2021; Schmitt et al., 2003; Tipper et al., 2006b; Tipper et al., 2010; Zhu and Macdougall, 1988). In several large rivers, small systematic seasonal variations in Ca isotopes and Mg/Ca ratios have been observed, with heavier Ca isotopic compositions and higher

Mg/Ca ratios during the dry season compared to the wet season, potentially indicating an important role for secondary mineral formation/dissolution (Tipper et al., 2010). In contrast, the reported seasonal variations in dissolved Mg isotopes in large river systems are negligible (Hindshaw et al., 2019; Mavromatis et al., 2020). Interestingly, studies in Arctic catchments suggest that inter-annual variations in both $\delta^{44/40}$Ca and δ^{26}Mg values have the potential to trace permafrost degradation (Hindshaw et al., 2019; Lehn et al., 2017), although data from other permafrost settings are required to assess the wider applicability of these findings. In the context of projected increases in the frequency of extreme precipitation and permafrost thawing due to global warming (Myhre et al., 2019; Wild et al., 2019), additional research into the behaviour of Ca and Mg isotopes in river water under various hydrological conditions is evidently required to determine the effect of climatic factors on the chemical weathering process.

The Tibetan Plateau is the source of 11 large rivers (Wu et al., 2009), and its temperature is rising twice as fast as the global average (Wang et al., 2021). This scenario makes it an ideal natural laboratory for evaluating the effect of climate on the water chemistry of large river systems. To explore the hydrological controls on chemical weathering, we measured $^{87}Sr/^{86}Sr$, $\delta^{44/40}$Ca, and δ^{26}Mg values in river water samples from both the Jinsha and Yalong rivers, two large rivers draining the eastern Tibetan Plateau, spanning one hydrological year. In combination with previous studies that reported on the spatial variation of these isotope systems in the same catchments (Chen et al., 2020; Ma et al., 2020; Zhang et al., 2019; Zhao et al., 2019), we attempt to determine the major processes that control the behaviour of Ca, Mg, and Sr isotopes

in the river waters. A better understanding of the seasonal response of Ca, Mg, and Sr isotopes to weathering processes serves to improve their use as weathering tracers, to advance our understanding of the mechanisms of chemical weathering, and to better assess the impact of climate change on elemental and isotopic fluxes to the oceans.

2 Research area

The Jinsha River, as one of the main tributaries of the Changjiang River, originates from the Jianggudiru Glacier on Mt. Geladandong at an altitude of 6621 m, drains an area of 340,000 km^2, and has a length of 2316 km (Lu et al., 2016). The catchment area of the Jinsha River above our sampling site is 264,810 km^2. The Yalong River is the largest tributary of the Jinsha River, originating from Mt. Bayan Kara at an altitude of 5000 m, with a length of 1571 km and a drainage area of 128,000 km^2 (Li et al., 2014). The fixed points used to monitor seasonal variations in river water chemistry were just upstream of the confluence of these two rivers near Panzhihua (Fig. 1a).

2.1 Topography

From their headwaters in the eastern Tibetan Plateau, the climate, slope, soil, and vegetation vary widely along the course of both the Jinsha and Yalong rivers. The Jinsha River can be divided into a source area, middle reaches, and lower reaches by the towns of Benzilan and Shigu, respectively, while the Yalong River is divided similarly by the city of Ganzi and the town of Dahewan (Fig. 1a). The source areas of the Jinsha and Yalong rivers are plateau terrains with very gentle slopes, which transition via sloping mountainous areas in the middle reaches to flat lowlands in the lower reaches (Li et al.,

156 2014; Ma et al., 2020). Soil depth increases with decreasing elevation, and the
157 vegetation ranges from alpine meadow in the source area, through arid and semi-arid
158 shrubs in the middle reaches, to a combination of coniferous forest and sub-tropical
159 forest in the lower reaches (Ren et al., 2016).

160 *2.2 Climate*

161 The study area is influenced by the Asian monsoon, with the climate varying
162 temporally from cold and dry in winter to warm and wet in summer, and spatially from
163 a cold-dry highland mountainous climate in the source areas and middle reaches to a
164 subtropical monsoon climate in the lower reaches (Noh et al., 2009; Zhong et al., 2021).
165 Both the Jinsha and Yalong catchments have a distinct wet season (June to October)
166 and dry season (November to May) (Wang et al., 2019) (Fig. 1c), which is conducive
167 to exploring changes in weathering processes under variable hydrological conditions.
168 The two fixed sampling sites are in the lower reaches of the Jinsha and Yalong rivers
169 (Fig. 1a), with temperatures during the sampling period varying from 5.9 to 34.6 °C,
170 with an average of 22.1 °C, based on the nearby weather station in Panzhihua (Fig. 1c).
171 The daily water discharge during a hydrologic year ranges from 353 to 6540 m^3/s for
172 the Jinsha River based on data from Panzhihua station, and from 399 to 8740 m^3/s for
173 the Yalong River based on data from Tongzilin station (2013-2014; Hydrological
174 Yearbook of the People's Republic of China). The precipitation is mainly concentrated
175 in the lower reaches of the catchment, contributing up to 70% of the total runoff. The
176 Jinsha and Yalong catchments experience distinct seasonal changes in hydrology, with
177 surface water mainly fed by rainfall during the wet monsoon season (June to October),

and recharged by groundwater and meltwater during the dry season (November to May) (Wang et al., 2019; Zhu, 2007).

2.3 Lithology

The source area of the Jinsha River contains evaporites (Fig. 1a) and is characterised by permafrost conditions (Fig. 1b), whereas neither is found in the source area of the Yalong River (Chen et al., 2020; Zhong et al., 2021). The middle sections of the Jinsha and Yalong rivers are dominated by low-grade Triassic metamorphic rocks (predominantly sandstones) that are intruded by granites, while the lower section is dominated by Palaeozoic carbonate rocks and Precambrian metamorphic rocks (Fig. 1a; Zhao et al., 2019). As the Jinsha and Yalong are large rivers and thus suitable for exploring weathering at a continental scale, a comparison between them will enable an assessment of the effects of specific inputs and influences (e.g. evaporites, permafrost) on river water chemistry and isotopes.

3 Sampling and methods

3.1 Sampling

The Jinsha and Yalong rivers were sampled just upstream of their confluence at Panzhihua (30 km and 20 km from Panzhihua, respectively; Fig.1a). Monthly sampling of river waters was conducted from November 2013 to October 2014, with increased sampling frequency during the monsoon period (Table 1). Water samples were collected from each river in pre-cleaned bottles. In the field, pH values and water temperature were measured. pH values and water temperature are measured by WTW3210 pH meter

(pH measurement accuracy is ± 0.01, temperature accuracy is ± 0.1), and EC is measured by lightning conductance meter (accuracy is ± 5%). All water samples were filtered through 0.45μm Millipore nitrocellulose membrane filters, titrated for alkalinity using HCl, packaged, and stored in clean bottles within 24 hours. Samples for major cations and trace elements were acidified with ultrapure HNO_3. The sampling methods for the water samples are described in detail in Zhong et al. (2021).

In addition, surface soil and bedload sediment samples from near the sampling sites of the Jinsha and Yalong rivers were collected during the wet season (August). The soil samples were collected from the river banks with a spade at a depth of 0-10 cm, and placed in a clean plastic bucket after removing plant material and stones. We gathered three random soil samples near the fixed river water sampling site for each river, and thoroughly mixed the three samples to make one uniform sample. The bedload sediment samples were collected using a scoop at depths ranging from 0 to 5 cm and transferred to pre-cleaned wide-mouth glass bottles. The sediment samples are primarily composed of river sand, with sediment particle sizes ranging from 0.125 to 0.5 mm, and more than half of them larger than 0.25 mm.

3.2 Soil and sediment leaching and digestions

After air drying the soils, ~10g was ground to *ca.* 200 mesh with an agate mortar, and then leached to isolate the carbonate and exchangeable fractions. The bedload sediment samples were treated in the same way. The leaching procedures followed Bagard et al. (2013): 1N acetic acid was used to obtain the carbonate phase, then 1N HCl was used to obtain the exchangeable phase, and finally 1N HNO_3 was used to

obtain the organic matter fraction (note that the leaching procedures cannot separate each phase quantitatively, and we expect that the 1N HCl leach may also attack the clay minerals). The leaching experiments were conducted at room temperature by reacting 1 g solid sample with 15 ml acid for 15 minutes with constant shaking. The mixtures were centrifuged at 7000 r/min, and the supernatants were filtered and collected in Teflon beakers. After each leaching step, the solid phase was rinsed three times with MQ water for 10 minutes, and the rinse liquids were added to the previously collected acid leachates. The leachates were dried at 100°C and re-dissolved in 2N HCl. In addition, bulk soil and bedload sediment powders were fully digested with concentrated HF and HNO_3.

3.3 Major and trace elements

For river water samples and soil/sediment leachates, major cations (Ca^{2+}, Mg^{2+}, Na^{+}, K^{+}, Si) and anions (Cl^{-}, NO_3^{-}, SO_4^{2-}) were determined by Inductively Coupled Plasma Optical Emission Spectrometry (ICP-OES, Vista MPX) and Ion Chromatography Dionex 90 (ICS-90), respectively. Concentrations of trace elements (Al, Sr, Fe, Rb, F) were measured by Inductively Coupled Plasma Mass Spectrometry (ICP-MS, Agilent 7900). The concentrations of ions were calibrated against a series of synthetic standard solutions, which were prepared gravimetrically from single element standard solutions (such as Ca, Mg, Na, K, Si, Li, Al, Rb, Sr, Fe) made in 3% HNO_3. During analysis, the MIX-3 standard was used as the monitor solution for the major elemental analysis and the MIX-4 standard was used for the minor elemental analysis. Both blank (3% HNO_3) and synthetic standard solutions (MIX-3 and MIX-4) were

measured every 5 samples to monitor drift. The external error (2SD) of the analysis is better than 5% for major elements, and better than 10% for minor elements.

3.4 Ca and Sr isotopes

Calcium and Sr were purified through one column using AG50W-X12 cation exchange resin. After eluting the matrix using 19 ml 2N HCl, Ca solutions were collected using 18 ml 2N HCl, and Sr solutions were then collected using 10 ml 3N HCl. After collection, Ca and Sr solutions were dried down and redissolved in concentrated HNO_3 three times, and finally dissolved in 0.3 M HNO_3 for analysis.

The Ca isotopic compositions ($^{44}Ca/^{42}Ca$) were measured by Nu Plasma HR Multicollector-Inductively Coupled Plasma Mass Spectrometer (MC-ICPMS) in the Isotope Geology Laboratory of the Chinese Academy of Geological Sciences. Isotopes of ^{42}Ca, ^{43}Ca, and ^{44}Ca were measured at low mass resolution. Analyses of $^{44}Ca/^{42}Ca$ and $^{43}Ca/^{42}Ca$ for samples were bracketed by measurements of the NIST 915b standard (Belshaw et al., 2000). Samples were diluted in 0.3 M HNO_3, ensuring that the ^{42}Ca intensity for samples and standards differed by less than 10%. In addition, a DSN 100 or CETAC Aridus desolvating nebulizer was used to reduce and stabilise the interferences (less than 2 mV for ^{42}Ca, ^{43}Ca, and ^{44}Ca). The detailed operating parameters for stable Ca isotope ratio measurement used in this study are listed in Table S1.

Calcium isotope values are reported in this study using the delta notation relative to the NIST SRM915a standard, as shown in equations (1) and (2).

$$\delta^{44/42}Ca_{915b}\ (‰) = \left[\frac{\left(\frac{^{44}Ca}{^{42}Ca}\right)_{sample} - \left(\frac{^{44}Ca}{^{42}Ca}\right)_{915b}}{\left(\frac{^{44}Ca}{^{42}Ca}\right)_{915b}}\right] \times 1000 \quad (1)$$

$$\delta^{44/42}Ca_{915a}\ (‰) = \delta^{44/42}Ca_{915b} + 0.35 \quad (2)$$

All samples were analysed 3 to 5 times per session, and the reported values are the mean of those measurements. Repeated analyses of NIST 915b gave a mean value of $\delta^{44/42}Ca_{915a}$ = 0.35 ± 0.05‰ (2sd, n = 21), in good agreement with literature values (Heuser and Eisenhauer, 2008; Hindshaw et al., 2011), and indicating an external analytical uncertainty of 0.05‰ (2sd) over the analysis period. Seawater (IAPSO) measured by this method yields $\delta^{44/42}Ca_{915a}$ values of 0.89 ± 0.05‰ (2sd, n = 5), in line with measurements from other studies that reported a long-term external analytical uncertainty of ± 0.05‰ (2sd) on $\delta^{44/42}$Ca values (Hippler et al., 2003; Pogge von Strandmann et al., 2019a). Other Ca isotope standards measured in this study were COQ-1, BHVO-2, BCR-2, GSR-3, AGV-2, and GSP-2. Their mean values and the corresponding long-term external two standard deviation (2SD), as well as measurements of the NIST 915b and IAPSO seawater standards, are summarised in Table S2. All these results are consistent with those reported in previous studies using high-precision double spike TIMS methods (He et al., 2017; Liu et al., 2017; Sun et al., 2021). Following the suggestion of Eisenhauer (2004), the Ca isotope results are expressed as $\delta^{44/40}$Ca relative to the standard NIST 915a, following the relationship in equation (3) (He et al., 2017):

$$\delta^{44/40}Ca_{915a} = 2.048 \times \delta^{44/42}Ca_{915a} \quad (3)$$

We apply ± 0.10‰ (2sd) as the external uncertainty on our sample $\delta^{44/40}$Ca values.

285 Radiogenic Sr isotopic compositions were measured by Thermo Neptune MC-
286 ICPMS at the School of Earth System Science, Tianjin University. ^{83}Kr and ^{85}Rb were
287 measured in order to correct for the isobaric interferences of ^{86}Kr and ^{87}Rb on ^{87}Sr
288 (following $^{86}Kr = 1.50566*^{83}Kr$ and $^{87}Rb = 0.3857*^{85}Rb$). Based on the exponential
289 mass bias law, the $^{87}Sr/^{86}Sr$ values were corrected using an $^{86}Sr/^{88}Sr$ ratio of 0.1194
290 (Weis et al., 2006). Repeated analyses of the NBS 987 standard interspersed with the
291 samples gave an $^{87}Sr/^{86}Sr$ ratio of 0.71027 ± 0.00002 (2sd, n = 40), in agreement with
292 previous studies (Bickle et al., 2018; Weis et al., 2006; Wu et al., 2009b). Based on the
293 good agreement of the NBS 987 standard with its true value, there was no need to apply
294 a correction to the Sr isotope data. Other Sr isotope standards measured in this study
295 were IAPSO, GSP-2, BCR-2, and COQ-1. Their mean values and the corresponding
296 long-term external two standard deviation (2SD), as well as measurements of the NIST
297 987 standard, are summarised in Table S3. All these results are consistent with those
298 reported in previous studies (Bellefroid et al., 2018; Ma et al., 2013; Weis et al., 2006).

299 *3.5 Mg isotopes*

300 The Mg isotopic compositions were measured in the recently-established LOGIC
301 (London Geochemistry and Isotope Centre) clean laboratory and mass spectrometer,
302 and we have therefore analysed a number of standards to assess accuracy and precision.
303 Samples for Mg isotope analysis were purified through a two-stage column procedure
304 using AG50W X-12 cation exchange resin, adapted from Pogge von Strandmann et al.
305 (2011). The first column used 2 M HNO_3 as an eluent, and the second column used 2
306 M HCl as an eluent, so as to completely separate both Ca and Fe from Mg. Splits were

307 collected before and after the Mg cut to test Mg concentrations. The combined splits
308 contained <0.5% of the sample Mg, showing that >99.5% of Mg was collected.
309 Samples were analysed using a Nu Plasma 3 MC-ICPMS following published
310 procedures (Pogge von Strandmann et al., 2011; Pogge von Strandmann et al., 2019b),
311 with a wet plasma setup to eliminate spectral interferences such as CN^+. With an uptake
312 rate of 100 ml/min and using the "low mass skimmer" from Nu Instruments, the beam
313 intensity was 100 pA total Mg for a 200 ng/g solution. The background (typically <0.1
314 pA) was subtracted from the sample intensity. The total procedural blank was <0.9 ng,
315 which is insignificant compared to the mass of Mg in the samples.
316 At least four secondary standards were processed through columns with each batch
317 of samples, and analyses were performed by sample-standard bracketing relative to the
318 standard DSM-3 (Galy et al., 2003). Magnesium isotope values are reported in this
319 study using the delta notation relative to the DSM-3 standard, as shown in equation (4).

320 $$\delta^{x}Mg = \left[\frac{\left(\frac{^{x}Mg}{^{24}Mg}\right)_{sample} - \left(\frac{^{x}Mg}{^{24}Mg}\right)_{standard}}{\left(\frac{^{x}Mg}{^{24}Mg}\right)_{standard}}\right] \times 1000 \quad (4)$$

321 Note that ^{x}Mg is either ^{25}Mg or ^{26}Mg. Seawater (IAPSO) and DSM-3 analysed during
322 the study gave $\delta^{26}Mg$ values of -0.82 ± 0.04‰ (2sd, n=11) and 0.02 ± 0.06 (2sd, n=14),
323 respectively, in agreement with previously published values (Pogge von Strandmann et
324 al., 2019a). The Cambridge-1 (CAM-1) standard gave a $\delta^{26}Mg$ value of -2.64 ± 0.07‰
325 (n=5), and the USGS BCR-2 standard gave a $\delta^{26}Mg$ value of -0.24 ± 0.08‰ (n=7), also
326 in agreement with other studies (see compilation in Pogge von Strandmann et al., 2011).
327 In a ^{26}Mg vs. ^{25}Mg cross plot (Fig. S1), all samples lie on a line with a slope of 0.523±

0.002, which is consistent with the theoretical equilibrium slope of 0.521 (Young and Galy, 2004). Therefore, both water and rock analyses appear to be accurate, and the long-term external analytical uncertainty of δ^{26}Mg values using this method and mass spectrometer is taken to be ± 0.08‰ (2sd).

3.6 Elemental flux calculations and concentration modelling

The LOADEST software, developed by the United States Geological Survey (USGS), was used to estimate constituent loads in rivers. Using continuous flow and discrete water quality monitoring data, the LOADEST model can automatically build up a statistical regression equation for daily river dissolved loads, which can then be estimated on a daily/monthly/seasonal/annual time scale. The software includes 9 models. In this study, AMLE was used to calculate the daily elemental concentrations and fluxes, and the detailed LOADEST settings used here are reported in Table S4.

4 Results

4.1 Hydrological conditions

Both the Jinsha and Yalong rivers have high and variable discharge during the wet season from July to September (Fig. 1 and 2, Table S5). The discharge then falls sharply between October and December due to low rainfall. The discharge of the Jinsha River reaches its minimum during the winter (from January to March) when the source river is frozen, and then increases slightly towards June as temperatures rise (Fig. 2, Table S5). For the Yalong River, there are rapid variations in discharge on monthly timescales during the dry season, which are not reproduced in the runoff of the Jinsha River during

the same period (Fig. 2, Table S5). This apparent flow anomaly may be related to seasonal reservoir regulation linked to the Er'tan Hydropower Station, the second-largest hydropower station in Asia, which is located 33 km upstream from our sampling site at the outlet of the Yalong River.

4.2 Temporal variability of river water chemistry and isotopic compositions

4.2.1 Variations of riverine elemental concentrations with discharge

The concentrations of major anions and cations (Zhong, 2017) in the Jinsha and Yalong river waters show variability during the hydrological year, as do concentrations of trace elements such as Sr, Fe, Al, and F (Fig. 2, Table 1). Moreover, the seasonal trends in concentrations differ between the two rivers.

The major soluble elements in the Jinsha River show broadly similar temporal patterns but with some differences in detail (Fig. 2a). For example, Ca, Mg, Na, K, SO_4, and Cl all show concentration peaks during both the pre-monsoon interval in June and during a post-monsoon interval, although the timing of the post-monsoon peak varies between elements (November to February). Similar seasonal trends are seen for minor elements such as Sr, F, and Fe (Fig. 2a, c). For most elements, the lowest concentrations are recorded during the monsoon interval, but for Na and Cl significantly lower values are reached in April to May (Fig. 2a, c).

For the Yalong River, major ion concentrations (Ca, Mg, Na, K, SO_4, and Cl) and Sr concentrations show similar patterns to each other, with gradual increases from October to May, followed by a steeper decrease in early July during the monsoon season (Fig. 2b and 2d). Unlike the Jinsha River, the peak concentrations occur later in the year

(around April to May) rather than in the post-monsoon interval and there is no distinct pre-monsoon peak in June (Fig. 2b and 2d). In general, the cation concentrations of the Yalong River follow a concentration-discharge relationship (Godsey et al., 2009) at low to moderate flows, indicating some effect of dilution (but offset above a theoretical dilution line), while the behaviour is closer to chemostatic during the high-water stage (Fig. 3b-d). Hence, the effect of dilution during the monsoon interval appears to be limited by enhanced contributions of solutes from other sources.

Additionally, both the Jinsha and Yalong rivers display similar trends in Al concentrations, which in both rivers show an increase during the monsoon season and a positive correlation with discharge (Fig. 2c, d). The concentrations of Si remain relatively constant through time in both the Jinsha and Yalong rivers (Fig. 3a), with such chemostatic behaviour potentially arising from an equilibrium between the river waters and secondary silicates (Clow and Mast, 2010; Torres et al., 2015).

4.2.2 Variations of riverine $^{87}Sr/^{86}Sr$ values

Both the Jinsha and Yalong river waters have less radiogenic $^{87}Sr/^{86}Sr$ values (0.71031-0.71086 and 0.71056-0.71192, respectively; Table 1) than Himalayan rivers (Boral et al., 2021; Tipper et al., 2006c). The $^{87}Sr/^{86}Sr$ values in the Jinsha River are relatively homogeneous, with a narrow range of variation during the whole hydrological year (Figs. 3f and 4a, Table 1). The greatest variation in $^{87}Sr/^{86}Sr$ values for the Jinsha River is during the low-water stage ($Q < 2000$ m^3/s) and is inversely related to discharge (Fig. 3f). During the high-water stage ($Q>4000$ m^3/s), the $^{87}Sr/^{86}Sr$ values are fairly constant, at around 0.71051 for the Jinsha River. The Yalong River also

393 shows a slightly greater range of $^{87}Sr/^{86}Sr$ values during the dry season (0.71056-
394 0.71177) than during the wet season (0.71095-0.71192) (Figs. 3f and Fig. 4b), but
395 displays a positive trend between $^{87}Sr/^{86}Sr$ values and discharge when Q < 2000 m^3/s
396 (Fig. 3f). During the high-water stage (Q>4000 m^3/s), the $^{87}Sr/^{86}Sr$ values are fairly
397 constant at around 0.71128 for the Yalong River (Fig. 3f).

398 *4.2.3 Variations of riverine $\delta^{44/40}Ca$ values*

399 The seasonal variation in $\delta^{44/40}Ca$ values of the Jinsha and Yalong rivers falls
400 within the range of spatial variation observed in the Jinsha and Yalong catchments
401 (Chen et al., 2020; Chen et al., 2022), but the relationship between $\delta^{44/40}Ca$ values and
402 discharge in the two rivers is different (Fig. 3g). For the Jinsha River, the $\delta^{44/40}Ca$ values
403 span a larger range from 0.78‰ to 1.17‰ (Fig. 3g, Table 1), displaying a positive trend
404 with discharge when Q < 2000m^3/s, then maintaining high values when 2000m^3/s < Q
405 < 4000m^3/s, followed by a negative trend with discharge when Q > 4000m^3/s (Fig. 3g).
406 Overall, the variation of $\delta^{44/40}Ca$ values in the Jinsha River is larger in the wet season
407 (0.78-1.17‰) than in the dry season (0.98-1.13‰). For the Yalong River, the $\delta^{44/40}Ca$
408 values fluctuate in a fairly narrow range between 0.71‰ and 0.95‰ (Fig. 3g, Table 1),
409 but show some interesting trends with discharge. Specifically, there is a negative
410 correlation between $\delta^{44/40}Ca$ values and discharge in the dry season (Q < 2000m^3/s),
411 and a positive correlation when 2000m^3/s < Q < 4000m^3/s, before values stabilise at
412 0.94‰ when Q > 4000m^3/s (Fig. 3g).

413 *4.2.4 Variations of riverine $\delta^{26}Mg$ values*

414 Both the Jinsha and Yalong rivers have $\delta^{26}Mg$ values that fall within the range of

global rivers (from -2.50‰ to +0.64‰, with a mean of -1.09‰) (Teng, 2017). The Jinsha River has a range of 0.27‰ (from -1.30‰ to -1.03‰) (Fig. 3h), which is much smaller than the spatial variation in river waters in the Jinsha catchment (-1.67‰ to -0.50‰) (Xu et al., 2022; Zhao et al., 2019). The Jinsha River δ^{26}Mg values are more variable during the dry season than during the wet season (Fig. 4a), increasing with discharge during the dry season (Q<2000m^3/s), then maintaining high values under intermediate to high flows (Q>2000m^3/s) (Fig. 3h). For the Yalong River, the δ^{26}Mg values have a slightly larger range of 0.39‰ (from -1.39‰ to -1.00‰). The Yalong River δ^{26}Mg values are more variable during the wet season than during the dry season (Fig. 4b), displaying a negative trend with discharge during both dry (Q<2000m^3/s) and wet seasons (Q>4000m^3/s) (Fig. 3h).

4.3 Leaching experiments

Table 2 reports the elemental ratios and isotopic compositions of the bedload sediment and soil leachates and digests. The carbonate fraction of the two soils (JSJA-1 and YLJA-1) have similar $\delta^{44/40}$Ca values (~0.50‰) and slightly different ^{87}Sr/^{86}Sr values (0.70997 and 0.71091). In contrast, the carbonate fraction of the river sediments (JSJN-1 and YLJN-1) yielded a wide range of $\delta^{44/40}$Ca values (0.54-0.79‰) and ^{87}Sr/^{86}Sr values (0.70957-0.71228). Considering the exchangeable fraction, the Sr isotopic composition of the soil on the banks of the two rivers (JSJA-2 and YLJA-2) is similar (~0.71200), but the Ca isotopic compositions are different (0.55 and 0.73‰). The exchangeable fraction of the two river sediments (JSJN-2 and YLJN-2) have similar ^{87}Sr/^{86}Sr values (~0.70980) and slightly different $\delta^{44/40}$Ca values (0.72‰ and

437 0.85‰). Furthermore, the $^{87}Sr/^{86}Sr$ values of the organic matter fractions in the soil and
438 river sediment samples are both higher than the $^{87}Sr/^{86}Sr$ values of the respective
439 carbonate and exchangeable fractions. This observation could indicate that the 1N
440 HNO_3 has also attacked some silicate mineral debris.

441 ## 5 Discussion

442 ### *5.1 Hydrological influences on chemical weathering rates*

443 Previous studies indicated that the Jinsha and Yalong rivers are dominated by
444 carbonate weathering (Ma et al., 2020; Noh et al., 2009; Wu et al., 2008), and that the
445 mainstream of the Jinsha is also impacted by evaporite dissolution in its source area
446 (Chen et al., 2020). A forward model following Noh et al. (2009) was used to calculate
447 the seasonal contributions from rainwater, silicates, carbonates, and evaporites (Table
448 S6). We then calculated the weathering rates in the study area, and also calculated ω_sil,
449 ω_carb, and ω_eva as the proportions of silicate, carbonate, and evaporite weathering
450 rates to total chemical weathering rates. The results are shown in Table S7, and details
451 of the calculation can be found in Figure S2.

452 For both the Jinsha and Yalong rivers, chemical weathering rates are higher in the
453 wet season than in the dry season (Fig. S3), while silicate weathering rates (SWR) are
454 lower than carbonate weathering rates (CWR) during the whole hydrologic year (Fig.
455 5a and 5b). The CWR in the wet season is up to 16 and 14 times higher than in the dry
456 season for the Jinsha and Yalong rivers, respectively (Fig. S3, Table S7). The CWR and
457 SWR of the Jinsha and Yalong rivers show subtle variations during the dry season, then

increase rapidly at the pre-monsoon stage (June), stay at relatively high levels during the monsoon interval (July to September), and then decrease sharply after the monsoon (October) (Table S7). Evaporite dissolution plays an important role in influencing the Jinsha river water chemistry (EWR: 5-212 t/km^2/y), whereas the EWR of the Yalong River is insignificant (3-20 t/km^2/y) (Fig. 5a and 5b, Fig. S3, Table S7). For the two rivers, although SWR are elevated during the wet monsoon season, ω_sil reaches a fairly stable minimum during this interval (Fig. 5a and 5b), in contrast to elevated ω_eva for the Jinsha and ω_carb for the Yalong.

5.2 Major solute sources to the Jinsha and Yalong

Even when the solute concentration behaviour is largely chemostatic (Fig. 3), changes in the sources of elements to river waters could still be occurring (Clow and Drever, 1996; Clow and Mast, 2010) and can potentially be traced using radiogenic Sr isotopes (Pett-Ridge et al., 2009). Previous studies on small watersheds have shown that longer water residence times during the dry season can lead to greater contributions from silicate versus carbonate weathering, which typically increases the riverine $^{87}Sr/^{86}Sr$ values, while increased carbonate dissolution during the wet season can lower $^{87}Sr/^{86}Sr$ values (Tipper et al., 2006c). However, this scenario is not entirely applicable to the large river catchments of this study. There is no significant seasonal relationship between riverine $^{87}Sr/^{86}Sr$ values and the ratio of SWR to CWR in either the Jinsha or Yalong river basins (Table S7). Therefore, seasonal changes in the relative contributions of silicate and carbonate weathering do not appear to be the main factor responsible for temporal variability in the $^{87}Sr/^{86}Sr$ values of these rivers.

Instead, mixing between different water sources under changing hydrological conditions may be the dominant control on the temporal variations in $^{87}Sr/^{86}Sr$ values (Calmels et al., 2011; Jacobson and Blum, 2000; Jacobson et al., 2002). This hypothesis is tested using mixing diagrams between $^{87}Sr/^{86}Sr$ values and elemental ratios (Fig. 6). Potential water sources include groundwater, meltwaters, and surface waters. Based on chemical composition, the surface waters can be divided into three types: the main tributaries of the two rivers which are dominated by carbonate weathering (Chen et al., 2022), the headwaters of the Jinsha river which are severely affected by evaporite dissolution (Chen et al., 2020), and the overland flow which reacts rapidly with topsoil during the monsoon season (Torres et al., 2015). The compositions of evaporites and soil leachates in the study area (Table 2) are taken to provide evidence on the chemical characteristics of the latter two water sources. Although time series samples of both the Jinsha and Yalong fall in a mixing region between meltwaters, evaporite-draining river waters, and soil leachates (grey area in Fig. 6), the contribution of groundwater cannot be ruled out. During the dry season, groundwater and meltwater are potential water sources due to the drying of the evaporite-dominated headwaters and the lack of overland flow to carry soil into the river system (Xie et al., 2018). As such, we consider that the river water sources differ depending on hydrological conditions, resulting in the seasonal variations in river water composition.

5.3 Controls during low-runoff periods: Meltwater and secondary mineral precipitation

During low-runoff periods ($Q < 2000$ m^3/s), the rivers are mainly recharged by

groundwater (Fig. 9a and b). Amorphous clay minerals can form within a few weeks in groundwaters that are forced out of equilibrium, at least to the extent that they can be detected by sensitive methods such as Mg isotopes (Oelkers et al., 2019). However, in the case of chemical equilibrium, the precipitation rates of crystalline clays tend to be much slower (Jacobson and Holmden, 2008; Jacobson et al., 2010). We therefore assume that seasonal variations in the chemistry and isotopic compositions of the groundwaters are mainly inherited from their hydrologic sources rather than from variability in in-situ water-rock interactions. In this scenario, the groundwater compositions are mainly affected by the infiltration of meltwaters during the dry season, and by river water recharge during the wet season, rather than representing a distinct source themselves.

5.3.1 Jinsha River basin: Permafrost meltwater and secondary carbonate precipitation

The source area of the Jinsha River is covered by permafrost (Fig. 1b), in which Ca-Mg sulphate salts are commonly formed (Cooper et al., 2002; Lehn et al., 2017; Rutter et al., 2011). From March onwards, as the permafrost begins to thaw, the dissolution of Ca-Mg sulphate salts dominates the chemical composition of the permafrost meltwater. Unfortunately, no samples of permafrost meltwater during the low-runoff period are available. Nonetheless, previous research has demonstrated that permafrost meltwater in the Jinsha source area and the Jinsha headwaters share the same water source (atmospheric precipitation) and solute source (Ca-Mg sulphate dissolution) (Ye and Chang, 2019). As a result, the $^{87}Sr/^{86}Sr$ value of the permafrost meltwater

should be comparable to that of the river at the Jinsha headwater (sample JS-1 in Chen et al., 2022). Due to the river drying, the headwaters of the Jinsha River are unable to provide solutes to the main stream during the low-runoff periods (Xie et al., 2018). At this point, the $^{87}Sr/^{86}Sr$ values in the Jinsha River decrease with increasing flow (Fig. 3f), which can only be attributed to permafrost meltwater input.

In addition, the Ca-Mg sulphate salts in the Jinsha source area have lower $\delta^{44/40}Ca$ (Chen et al., 2020) and similar $\delta^{26}Mg$ values (Zhao et al., 2019) compared to the river water samples collected during low-runoff periods (Table 2). As a result, the increase in the $\delta^{44/40}Ca$ and $\delta^{26}Mg$ values with increasing flow in the Jinsha River (Fig. 3g and 3h) cannot be explained solely by the dissolution of the Ca-Mg sulphate salts. Instead, the Ca-Mg isotopes in the permafrost meltwater could be fractionated by other processes. Previous studies have suggested that secondary carbonate precipitation, clay adsorption, and cation exchange preferentially take up lighter Ca and Mg isotopes (Brazier et al., 2019; Cenki-Tok et al., 2009; Jacobson and Holmden, 2008; Nelson et al., 2021; Teng, 2017; Tipper et al., 2006a). In contrast, plant growth preferentially takes up heavy Mg as well as light Ca isotopes (Black et al., 2008; Bolou-Bi et al., 2010; Bolou-Bi et al., 2012; Nelson et al., 2022; Page et al., 2008; Schmitt et al., 2003; Wiegand, 2005), resulting in liquid phases having light Mg and heavy Ca isotopic compositions, which is inconsistent with the patterns observed for $\delta^{44/40}Ca$ and $\delta^{26}Mg$ values in Jinsha River waters (Fig. 8b). Hence, vegetation is not the controlling factor driving Ca-Mg isotope fractionation. Although we cannot rule out effects from clay adsorption or cation exchange, the positive correlations between $\delta^{44/40}Ca$ values and

Sr/Ca ratios (Fig. 7c), and the positive correlation between δ^{26}Mg values and the dolomite saturation index (DSI) (Fig. 8d, Table S8) for the Jinsha River in the dry season, suggest that secondary carbonate precipitation plays an important role in fractionating Ca and Mg isotopes (Fig. 9a). Previous studies have also demonstrated that Ca and Mg removal by secondary carbonate precipitation is common in eastern Tibetan and Himalayan river catchments (Bickle et al., 2005; Bickle et al., 2018; Chen et al., 2020; Jacobson et al., 2002; Tripathy et al., 2010; Zhao et al., 2019), so our interpretation appears reasonable.

In permafrost regions, increasing air temperatures deepen the seasonally-thawed zone, leading to the dissolution of Ca-Mg sulphate salts. Consequently, carbonate saturation indices are elevated, facilitating carbonate precipitation, and thereby increasing the dissolved $\delta^{44/40}$Ca and δ^{26}Mg values in the Jinsha River basin (Fig. 9a). In addition, the δ^{26}Mg values in the Jinsha river waters exhibit a negative correlation with $^{87}Sr/^{86}Sr$ (Fig. 8a) and also show a positive correlation with chemical ratios indicating evaporite contributions, such as SO_4/Mg (Fig. S4d). Further, although the variations may be negligible when considering analytical error ($\pm$0.10‰), a general positive correlation between temperature and $\delta^{44/40}$Ca values in the Jinsha River is observed during the dry season (Fig. 7d), which is also consistent with the operation of secondary carbonate precipitation.

5.3.2 Yalong River basin: Snow meltwater and secondary silicate formation

Unlike the Jinsha River, the Yalong River is not influenced by evaporite

dissolution (Fig. 1) (Chen et al., 2022; Ma et al., 2020). The $^{87}Sr/^{86}Sr$ values in the Yalong river waters increase with increasing discharge during the dry period (Fig. 3f), which can be attributed to an increasing input of snow meltwater (Fig. 6). In addition, the $\delta^{26}Mg$ values of the Yalong River show a negative correlation with illite saturation indices (ISI) (Fig. 8c) in the low-runoff season, implying that the formation of clay minerals dominates the Mg isotopic composition of the river waters. Even though the direction of Mg isotope fractionation for clay minerals is not uniform (Brewer et al., 2018; Hindshaw et al., 2020; Pogge von Strandmann et al., 2008; Ryu et al., 2016; Wimpenny et al., 2010), experimental data indicate that the formation of Mg-rich clay minerals (e.g. illite and montmorillonite) preferentially incorporates ^{26}Mg, causing the residual solutions to be enriched in ^{24}Mg (Wimpenny et al., 2014; Wimpenny et al., 2010). Illite is the most abundant clay mineral in the suspended particulate matter and river sediments of the upper Changjiang River (Ding et al., 2013) and the ISI of the Yalong River shows a positive correlation with discharge during the low-runoff period (Fig. S4 and Table S8). We therefore suggest that meltwaters may wash out "old" waters from the soil, which had developed lower $\delta^{26}Mg$ values due to illite precipitation during the dry season (Fig. 9b), such that the soil water partly controls the Mg isotopic composition of the Yalong river waters during the dry season. Alternatively, since meltwater seeps through the soil and into the groundwater that recharges the river waters, we cannot rule out the possibility of secondary illite formation occurring in the groundwater. Future monitoring of the chemical composition of groundwater and soil water may aid in determining the location of secondary mineral formation in such

589 systems.

590 Compared with the Jinsha River, the Yalong River shows a narrower range of
591 $\delta^{44/40}$Ca values during the hydrological year and does not show a significant correlation
592 between $\delta^{44/40}$Ca values and SO_4/Ca ratios, CSI, or discharge during the dry season (Fig.
593 7). This differing pattern could be attributed to reservoir operations, which release dam
594 water to increase the water discharge during the low-runoff periods (Wang et al., 2019).
595 Dam-released water has a lower pH value and temperature than river water, making it
596 undersaturated for carbonates (Négrel et al., 2021; Wang et al., 2022). As a result, when
597 dam water enters the river, it can be expected to reduce carbonate saturation and inhibit
598 secondary carbonate precipitation. The carbonate saturation indices of the Yalong River
599 decrease with increasing discharge during the low-runoff period (Fig. S4a and 4b),
600 which might indicate the input of water released from the reservoir. For the Yalong river
601 water, carbonates change from supersaturated to undersaturated (Fig. S4a), which
602 would presumably result in the dissolution of some of the previously precipitated
603 secondary carbonates. Secondary carbonate precipitation preferentially uptakes the
604 lighter Ca and Mg isotopes (Tipper et al., 2006a), so their dissolution would decrease
605 the Ca and Mg isotopic compositions of the Yalong river water (Fig. 3g and 3h).
606 Because Sr is rarely found in secondary carbonates (Stewart et al., 1998), the $^{87}Sr/^{86}Sr$
607 values of the Yalong river waters are not affected by the secondary carbonate
608 dissolution. In conclusion, the changing trend of the carbonate saturation index, Ca and
609 Mg isotopic compositions during the low-runoff period in the Yalong River may
610 indicate the influence of hydrological regulation due to dam construction.

In summary, as the air temperature increases during the dry season, some of the meltwater might infiltrate the soil and wash out the aged soil solution, which in turn affects river water chemistry. Meanwhile, some of the meltwater might infiltrate into groundwater, indirectly affecting the chemical composition of the river water by regulating the composition of the groundwater. The Jinsha River is mainly recharged by permafrost meltwaters during the dry season (Fig. 9a), whereas the Yalong River is fed by meltwaters from snow and glaciers and dam waters (Fig. 9b). These high-relief large river systems might preserve the Sr, Ca, and Mg isotope signatures of recharge meltwaters that interacted with soil porewaters and groundwater, where both Ca and Mg isotopes are fractionated by the precipitation of secondary minerals i.e. carbonates in the case of the Jinsha River, and silicates in the case of the Yalong River (Fig. 9a and 9b).

5.4 Controls during medium-runoff periods: Tributary mixing and rock weathering

When the intensity of precipitation is greater than the soil infiltration capacity, the rainwater that exceeds the infiltration capacity forms surface runoff (Yang et al., 2014). During these times of increasing discharge, we hypothesise that the chemical composition of the Jinsha and Yalong rivers are dominated by the mixing of waters from the tributaries and the unfrozen headwaters, which carry rock weathering information from these sub-catchments (Fig. 9c and 9d). Such source mixing is thought to be the main cause of seasonal variations in the chemical composition of many large river systems, including the Ganga and Brahmaputra (Bickle et al., 2003; Boral et al., 2021), the Irrawaddy and Salween (Chapman et al., 2015), and the lower Changjiang

633 River (Luo et al., 2014).

634 In the range of 2000$m^3/s < Q < 4000m^3/s$, the weathering proportions of each rock
635 endmember in the Jinsha and Yalong rivers are insensitive to discharge (Fig. S3).
636 Compared to the dry season, the proportion of evaporite weathering in the Jinsha river
637 basin is higher (average value of samples from July to September: 35%), and the
638 proportion of silicate (26%) and carbonate (39%) weathering is lower (Fig. 5a, Fig. S3,
639 Table S7). During these periods, the $^{87}Sr/^{86}Sr$, $\delta^{44/40}Ca$, and $\delta^{26}Mg$ values in the Jinsha
640 river waters are similar to those of the headwaters, which are influenced by evaporite
641 dissolution (Fig. 6, 7, and 8), indicating that the evaporite-dominated source rivers
642 govern the water chemistry and isotopic compositions of the Jinsha River (Fig. 9c).
643 This finding is consistent with previous research on the spatial variation of isotopes
644 during summer seasons, which showed that evaporite weathering controls the Li (Ma
645 et al., 2020), Mg (Zhao et al., 2019), Ca, and Sr isotopic compositions (Chen et al.,
646 2020; Chen et al., 2022) of the Jinsha mainstream. For the Yalong River, the proportion
647 of carbonate weathering (average value of samples from July to September: 70%) is
648 slightly higher during these wetter periods compared to the dry season, and the
649 proportion of silicate (27%) and evaporite weathering (2%) is slightly lower (Fig. 5b,
650 Fig. S3, Table S7), indicating greater carbonate dissolution relative to silicate
651 weathering during this period. Apart from the source area of the Jinsha River,
652 carbonates are widely distributed in both the Jinsha and Yalong river basins (Fig. 1a),
653 and the water chemistry of most of their tributaries is dominated by carbonate
654 weathering (Chen et al., 2020; Ma et al., 2020; Zhang et al., 2019). Carbonates have

655 relatively lower $^{87}Sr/^{86}Sr$, $\delta^{44/40}Ca$, and $\delta^{26}Mg$ values than silicates (Table 2), and
656 therefore the decreases in $^{87}Sr/^{86}Sr$, $\delta^{44/40}Ca$, and $\delta^{26}Mg$ values in the Yalong river
657 waters as discharge increases in the range of $2000m^3/s<Q<4000m^3/s$ (Fig. 3f-h) could
658 be attributed to inputs from carbonate-dominated tributaries (Fig. 9d).

659 In summary, we suggest that the increase in precipitation during the intermediate-
660 flow periods increases the catchment area in the whole catchment, which might induce
661 more rock weathering. The chemical composition of the Jinsha River is dominated by
662 inputs from evaporite-dominated surface flow (Fig. 9c), whereas the Yalong River
663 water is governed by inputs from carbonate-dominated surface flow (Fig. 9d).

664 *5.5 Controls during the high-runoff period: Rapid surface flow and soil weathering*

665 Based on research in watershed hydrology, overland flow is generated during
666 heavy rainfall periods and flows through gullies into the river network (Yang et al.,
667 2014). Such overland flows can also erode surface soils, and thereby carry both soil
668 debris and soil water into the rivers. In previous studies, the weathering of soil minerals
669 has been shown to impact river water chemical compositions during monsoon
670 conditions (Bagard et al., 2011; Gurumurthy et al., 2015; Wei et al., 2013). We therefore
671 suggest that soil weathering may contribute to the dissolved solutes in the Jinsha and
672 Yalong river waters during the heavy rainfall period ($Q>4000m^3/s$). Support for a
673 surface soil input also comes from a recent study on the same river water samples,
674 which showed that dissolved organic carbon (DOC) concentrations increase during the
675 storm periods (Zhong et al., 2021).

676 *5.5.1 Exchange reactions*

It was recently demonstrated that the chemistry of the exchange pool on suspended particulate matter is in exchange equilibrium with river water in a series of global rivers (Tipper et al., 2021). In this case, we hypothesize that changes in the chemical composition of the river waters during the high-runoff period could be caused by inputs from the soil exchange pool. During the high-runoff period, the $^{87}Sr/^{86}Sr$ values in the Jinsha and Yalong river waters (Table 1, Jinsha: 0.71038-0.71065; Yalong: 0.71114-0.71155) are higher than in the exchangeable fraction of the riverbed sediments collected from this period (Table 2, JSJN-2: 0.70978 and YLJN-2: 0.70990). Since the relative contributions from different lithologies appears to have been almost constant (Fig. 5), the input of Sr from the soil exchange pool with a high Sr isotopic composition (Table 2, ~ 0.71200) could provide a possible solution.

In addition, Ca isotope data also support a soil exchange pool input during the high-runoff period. For the Yalong River, the $\delta^{44/40}Ca$ value of the soil exchangeable fraction (0.73±0.10‰) is consistent with the $\delta^{44/40}Ca$ value of the river water (Table 2, ~0.90±0.10‰) and the exchangeable fraction of the river sediment (0.85±0.10‰), within analytical uncertainty. Therefore, the input of Ca from the soil exchange reservoir would not cause a significant change in the $\delta^{44/40}Ca$ value of the river, which is consistent with the $\delta^{44/40}Ca$ value of the Yalong River being stable at 0.90‰ during the high-runoff period (Fig. 3g, Fig. 4b). For the Jinsha River, the $\delta^{44/40}Ca$ value of the soil exchangeable fraction (0.55±0.10‰) is lower than that of the river water (0.78-1.14‰), so with the increase of soil reservoir input, the $\delta^{44/40}Ca$ value of river water would be expected to gradually decrease, as observed (Fig. 3g, Fig. 4a).

699 *5.5.2 Dissolution of secondary soil minerals*

700 Secondary minerals such as pedogenic carbonates precipitate in soils following
701 previous flood events and can then be washed into rivers and re-dissolved during the
702 wet season (Huth et al., 2019; Kajita et al., 2020; Meyer et al., 2014). Unlike the almost
703 constant radiogenic Sr isotopes, the $\delta^{44/40}$Ca values in the Jinsha River system decrease
704 with increasing discharge during the high-runoff period (Fig. 3g). In addition to the
705 input of the soil exchange pool mentioned above (Section 5.5.1), another possible
706 explanation is that the input of Ca from secondary carbonates in soils (Table 2, JSJA-
707 1) could lower the $\delta^{44/40}$Ca values of river water, while having no significant impact on
708 the riverine $^{87}Sr/^{86}Sr$ composition, since secondary calcite has a low Sr concentration
709 (Tesoriero and Pankow, 1996). Compared with the Jinsha River, the dissolution of
710 secondary carbonates in soil has less impact on the Yalong River (Fig. 3g), which may
711 be an expected consequence of the limited production of secondary carbonates in the
712 Yalong River basin (Chen et al., 2022). In addition to secondary carbonates, the constant
713 dissolved Si concentrations throughout the hydrological year in both rivers suggests a
714 buffering by the precipitation and dissolution of secondary silicates (Fig. 3a) (Clow and
715 Mast, 2010; Georg et al., 2006; Torres et al., 2015). Since Ca is the dominant element
716 in carbonates but a trace element in clay minerals, we expect the weathering of
717 secondary silicates to have little effect on the riverine $\delta^{44/40}$Ca values (Nelson et al.,
718 2022).

719 The effects of both secondary mineral precipitation and exchange reactions on
720 riverine Mg isotopes remain controversial. While secondary carbonates preferentially
721 take up light Mg isotopes (Mavromatis et al., 2013; Oelkers et al., 2018; Pearce et al.,

722 2012; Schott et al., 2016), the direction of Mg isotope fractionation during clay mineral
723 formation is controlled by the mineral type, structure, and solution conditions (Chapela
724 Lara et al., 2017; Hindshaw et al., 2020; Pogge von Strandmann et al., 2008).
725 Furthermore, illite preferentially adsorbs light Mg isotopes, resulting in higher δ^{26}Mg
726 values in solution (Wimpenny et al., 2014), whereas gibbsite and Fe-(hydr)oxides
727 preferentially adsorb ^{26}Mg, resulting in lower solution δ^{26}Mg values (Chapela Lara et
728 al., 2017; Liu et al., 2014). In the Jinsha and Yalong river basins, illite is the most
729 abundant clay mineral, but the increase in Al and Fe concentrations when Q>4000m^3/s
730 (Table 1) could also be related to the input (and dissolution) of gibbsite and Fe-
731 (hydr)oxides during storms (Bagard et al., 2011). Therefore, the effects of adsorption
732 by different clay minerals and oxides on Mg isotopes in the river waters may
733 approximately cancel out. For both rivers, the Mg isotope data from the monsoon
734 season show a limited range of values (Fig. 4), which suggests that any fractionation is
735 minor, making it hard to resolve the possible effects of cation exchange or secondary
736 mineral dissolution based on Mg isotopes. However, the observed correlations between
737 δ^{26}Mg and ^{87}Sr/^{86}Sr values throughout the hydrological year (Fig. 8a) seem to indicate
738 that lithology is the primary control on seasonal variations in riverine δ^{26}Mg values.
739 To summarise, rapid overland flow transfers large amounts of soil into the river
740 during the monsoon season (Q>4000m^3/s), with soil weathering playing an important
741 role in regulating river water chemistry and isotope values during these times (Fig. 9e
742 and 9f). Variability in $\delta^{44/40}$Ca and ^{87}Sr/^{86}Sr values in the river waters are attributed to a
743 combination of secondary mineral dissolution of carbonates (and potentially

744 aluminosilicates) and exchange reactions (Fig. 9e and 9f).

745 6 Conclusions

746 In order to provide a better understanding of the effects of hydrological processes
747 on chemical weathering in large river systems, we studied temporal variations in river
748 water chemistry and $^{87}Sr/^{86}Sr$, $\delta^{44/40}Ca$, and $\delta^{26}Mg$ values in the Jinsha and Yalong river
749 waters. Temporal variations in the river water chemistry and isotopic compositions are
750 attributed to differences in the flow paths, source material being weathered, and
751 accompanying secondary processes under different hydrological conditions.

752 During the low-runoff period ($Q<2000 m^3/s$), meltwater seeps through the soil and
753 into the groundwater that recharges the river. The chemical compositions of both the
754 Jinsha and Yalong river waters are therefore governed by the chemical composition of
755 the soil water and groundwater, which is affected by permafrost meltwater in the Jinsha
756 river basin and by glacial meltwater in the Yalong river basin.

757 During the medium-runoff period ($2000 m^3/s<Q<4000 m^3/s$), rainwater interacts
758 with bedrock and the contribution of bedrock chemical weathering (relative to soil
759 water and groundwater inputs) to river water chemistry increases. During this period,
760 the mainstream water chemistry and isotopic compositions are dominated by the inputs
761 from the tributaries and headwaters. The evaporite-dominated headwater governs the
762 water chemistry and isotopic compositions in the Jinsha River, whereas the Yalong
763 River is governed by carbonate-dominated tributaries.

764 During the high-runoff period ($Q>4000 m^3/s$), heavy rainfall leads to rapid surface

765 flow, which transports a large volume of soil minerals into the Jinsha and Yalong river
766 waters. Those minerals include both secondary carbonates and clays, which regulate
767 river water chemistry through mineral dissolution and cation exchange. Dissolution of
768 amorphous aluminosilicates during heavy rainfall intervals could contribute to the
769 chemical stability of Si, which may in turn inhibit the weathering of primary silicate
770 minerals. In addition, Na ions can be released from soil-derived clays into river water
771 through cation exchange. Therefore, while silicate weathering fluxes are observed to
772 increase during the wet monsoon season, coeval increases in cation exchange could
773 result in an over-estimation of the magnitude of the increase in silicate weathering rate
774 and its CO_2 consumption when conventional approaches are applied. In the context of
775 projected increases in the frequency of extreme precipitation due to global warming,
776 our observations suggest that the impact of hydrological events on chemical weathering
777 fluxes and carbon cycling requires further consideration.
778
779 **Acknowledgements**
780 This work was funded by the 2nd Tibetan Plateau Scientific Expedition and Research
781 (2019QZKK0707), the Tianjin Science Fund for Distinguished Young Scholars
782 (18JCJQJC46200), the National Natural Science Foundation of China (41925002), and
783 the UK-China Joint Research and Innovation Partnership Fund PhD Placement
784 Programme (201806250237). PPvS was funded by ERC Consolidator grant 682760
785 CONTROLPASTCO2. DJW was supported by a NERC independent research
786 fellowship (NE/T011440/1). We thank Xu-Nan Meng, Li-Xin Zhang, and Peng-Fei Li
787 at Tianjin University for help with Sr isotope analysis, and Sen Xu for support in

LOADEST software. We also thank the associate editor Andrew Jacobson and three anonymous reviewers for their constructive comments. For the purpose of open access, the author has applied a 'Creative Commons Attribution (CC BY) licence' to any Author Accepted Manuscript version arising.

Appendix A. Supplementary Material

Supplementary data (Figures S1-S4 and Tables S1-S8) to this article can be found online. Fig. S1. shows magnesium three-isotope diagram for samples analysed in this study. Fig. S2. shows the forward model used to calculate the contribution of different endmembers to the river waters. Fig. S3. shows relationships between discharge and a range of chemical weathering parameters. Fig. S4. shows relationships of (a) dolomite saturation index (DSI), (b) calcite saturation index (CSI), and (c) illite saturation index (ISI) with discharge in the Jinsha (JS) and Yalong (YL) rivers. (d) Relationship between $\delta^{26}Mg$ values and SO_4/Mg ratios. Table S1 shows detailed operating parameters for stable Ca isotope ratio measurement using Nu Plasma HR MC-ICPMS in this study. Table S2 shows stable Ca isotopic composition of geological reference materials from this study. Table S3 shows $^{87}Sr/^{86}Sr$ values of geological reference materials from this study. Table S4 shows detailed LOADEST program settings used for concentration and flux calculations. Table S5 shows monthly average discharge and suspended particulate matter content in the Jinsha and Yalong rivers. Table S6 shows contribution of different endmembers to river water chemistry. Table S7 shows seasonal variations in chemical weathering rates and proportions for different lithologies.

References

Bagard, M.-L., Anne-Désirée Schmitt, François Chabaux, Oleg S. Pokrovsky, Jérôme Viers, Peter Stille, François Labolle, Anatoly S. Prokushkin, 2013. Biogeochemistry of stable Ca and radiogenic Sr isotopes in a larch-covered permafrost-dominated watershed of Central Siberia. Geochimica et Cosmochimica Acta 114, 169-187.

Bagard, M.-L., François Chabaux, Oleg S. Pokrovsky, Jérome Viers, Anatoly S. Prokushkin, Peter Stille, Sophie Rihs, Anne-Désirée Schmitt, Bernard Dupré, 2011. Seasonal variability of element fluxes in two Central Siberian rivers draining high latitude permafrost dominated areas. Geochimica et Cosmochimica Acta 75, 3335-3357.

Bellefroid, E.J., Planavsky, N.J., Miller, N.R., Brand, U., Wang, C., 2018. Case studies on the utility of sequential carbonate leaching for radiogenic strontium isotope analysis. Chemical Geology 497, 88-99.

Belshaw, N., Zhu, X., Guo, Y., O'Nions, R., 2000. High precision measurement of iron isotopes by plasma source mass spectrometry. International Journal of Mass Spectrometry 197, 191-195.

Berner, E.K., Berner, R.A., 2012. Global environment: water, air, and geochemical cycles. Princeton University Press.

Berner, R.A., 1997. The Rise of Plants and Their Effect on Weathering and Atmospheric CO_2. Science 276, 544-546.

Bickle, M.J., Bunbury, J., Chapman, H.J., Harris, N.B.W., Fairchild, I.J., Ahmad, T., 2003. Fluxes of Sr into the headwaters of the Ganges. Geochimica et Cosmochimica Acta 67, 2567-2584.

Bickle, M.J., Chapman, H.J., Bunbury, J., Harris, N.B.W., Fairchild, I.J., Ahmad, T., Pomiès, C., 2005. Relative contributions of silicate and carbonate rocks to riverine Sr fluxes in the headwaters of the Ganges. Geochimica et Cosmochimica Acta 69, 2221-2240.

Bickle, M.J., Chapman, H.J., Tipper, E., Galy, A., De La Rocha, C.L., Ahmad, T., 2018. Chemical weathering outputs from the flood plain of the Ganga. Geochimica et Cosmochimica Acta 225, 146-175.

Black, J.R., Epstein, E., Rains, W.D., Yin, Q.-Z., Casey, W.H., 2008. Magnesium-Isotope Fractionation During Plant Growth. Environmental Science & Technology 42, 7831-7836.

Bolou-Bi, E.B., Poszwa, A., Leyval, C., Vigier, N., 2010. Experimental determination of magnesium isotope fractionation during higher plant growth. Geochimica et Cosmochimica Acta 74, 2523-2537.

Bolou-Bi, E.B., Vigier, N., Poszwa, A., Boudot, J.-P., Dambrine, E., 2012. Effects of biogeochemical processes on magnesium isotope variations in a forested catchment in the Vosges Mountains (France). Geochimica et Cosmochimica Acta 87, 341-355.

Boral, S., Peucker-Ehrenbrink, B., Hemingway, J.D., Sen, I.S., Galy, V., Fiske, G.J., 2021. Controls on short-term dissolved $^{87}Sr/^{86}Sr$ variations in large rivers: Evidence from the Ganga–Brahmaputra. Earth and Planetary Science Letters 566, 116958.

Brazier, J.-M., Schmitt, A.-D., Gangloff, S., Pelt, E., Chabaux, F., Tertre, E., 2019. Calcium isotopic fractionation during adsorption onto and desorption from soil phyllosilicates (kaolinite, montmorillonite and muscovite). Geochimica et Cosmochimica Acta 250, 324-347.

Brewer, A., Teng, F.-Z., Dethier, D., 2018. Magnesium isotope fractionation during granite weathering. Chemical Geology 501, 95-103.

Calmels, D., Galy, A., Hovius, N., Bickle, M., West, A.J., Chen, M.-C., Chapman, H., 2011. Contribution

of deep groundwater to the weathering budget in a rapidly eroding mountain belt, Taiwan. Earth and Planetary Science Letters 303, 48-58.

Cenki-Tok, B., Chabaux, F., Lemarchand, D., Schmitt, A.-D., Pierret, M.-C., Viville, D., Bagard, M.-L., Stille, P., 2009. The impact of water–rock interaction and vegetation on calcium isotope fractionation in soil- and stream waters of a small, forested catchment (the Strengbach case). Geochimica et Cosmochimica Acta 73, 2215-2228.

Chao, H.-C., You, C.-F., Liu, H.-C., Chung, C.-H., 2015. Evidence for stable Sr isotope fractionation by silicate weathering in a small sedimentary watershed in southwestern Taiwan. Geochimica Et Cosmochimica Acta 165, 324-341.

Chapela Lara, M., Buss, H.L., Pogge von Strandmann, P.A.E., Schuessler, J.A., Moore, O.W., 2017. The influence of critical zone processes on the Mg isotope budget in a tropical, highly weathered andesitic catchment. Geochimica et Cosmochimica Acta 202, 77-100.

Chapman, H., Bickle, M., Thaw, S.H., Thiam, H.N., 2015. Chemical fluxes from time series sampling of the Irrawaddy and Salween Rivers, Myanmar. Chemical Geology 401, 15-27.

Chen, B.-B., Li, S.-L., Pogge von Strandmann, P.A.E., Sun, J., Zhong, J., Li, C., Ma, T.-T., Xu, S., Liu, C.-Q., 2020. Ca isotope constraints on chemical weathering processes: Evidence from headwater in the Changjiang River, China. Chemical Geology 531, 119341.

Chen, B.-B., Li, S.-L., Pogge von Strandmann, P.A.E., Wilson, D.J., Zhong, J., Sun, J., Liu, C.-Q., 2022. Calcium isotopes tracing secondary mineral formation in the high-relief Yalong River Basin, Southeast Tibetan Plateau. Science of The Total Environment 827, 154315.

Chetelat, B., Liu, C.Q., Zhao, Z.Q., Wang, Q.L., Li, S.L., Li, J., Wang, B.L., 2008. Geochemistry of the dissolved load of the Changjiang Basin rivers: Anthropogenic impacts and chemical weathering. Geochimica et Cosmochimica Acta 72, 4254-4277.

Clow, D.W., Drever, J.I., 1996. Weathering rates as a function of flow through an alpine soil. Chemical Geology 132, 131-141.

Clow, D.W., Mast, M.A., 2010. Mechanisms for chemostatic behavior in catchments: Implications for CO_2 consumption by mineral weathering. Chemical Geology 269, 40-51.

Cooper, R.J., Wadham, J.L., Tranter, M., Hodgkins, R., Peters, N.E., 2002. Groundwater hydrochemistry in the active layer of the proglacial zone, Finsterwalderbreen, Svalbard. Journal of Hydrology 269, 208-223.

Deng, K., Yang, S., Guo, Y., 2022. A global temperature control of silicate weathering intensity. Nature Communications 13, 1781.

Dessert, C., Lajeunesse, E., Lloret, E., Clergue, C., Crispi, O., Gorge, C., Quidelleur, X., 2015. Controls on chemical weathering on a mountainous volcanic tropical island: Guadeloupe (French West Indies). Geochimica et Cosmochimica Acta 171, 216-237.

Ding, T.-P., Gao, J.-F., Shi, G.-Y., Chen, F., Wang, C.-Y., Han, D., Luo, X.-R., 2013. The contents and mineral and chemical compositions of suspended particulate materials in the Yangtze River, and their geological and environmental implacations. Acta Geologica Sinica 87, 634-660 (*In Chinese with English abstract*).

Eisenhauer, A., Nagler, T., Stille, P., Kramers, J., Gussone, N., Bock, B., Fietzke, J., Hippler, D., Schmitt, A.-D., 2004. Proposal for International Agreement on Ca Notation Resulting from Discussions of Workshops on Stable Isotope Measurements Held in Davos (Goldschmidt 2002) and Nice (EGS-AGU-EUG 2003). Geostandards Newsletter 28, 149-152.

Ewing, S.A., Yang, W., DePaolo, D.J., Michalski, G., Kendall, C., Stewart, B.W., Thiemens, M.,

Amundson, R., 2008. Non-biological fractionation of stable Ca isotopes in soils of the Atacama Desert, Chile. Geochimica et Cosmochimica Acta 72, 1096-1110.

Fan, B., Zhao, Z.-Q., Tao, F., Li, X., Tao, Z., Gao, S., He, M., 2016. The geochemical behavior of Mg isotopes in the Huanghe basin, China. Chemical Geology 426, 19-27.

Fantle, M.S., Tipper, E.T., 2014. Calcium isotopes in the global biogeochemical Ca cycle: Implications for development of a Ca isotope proxy. Earth-Science Reviews 129, 148-177.

Fries, D.M., James, R.H., Dessert, C., Bouchez, J., Beaumais, A., Pearce, C.R., 2019. The response of Li and Mg isotopes to rain events in a highly-weathered catchment. Chemical Geology 519, 68-82.

Galy, A., Yoffe, O., Janney, P.E., Williams, R.W., Cloquet, C., Alard, O., Halicz, L., Wadhwa, M., Hutcheon, I.D., Ramon, E., Carignan, J., 2003. Magnesium isotope heterogeneity of the isotopic standard SRM980 and new reference materials for magnesium-isotope-ratio measurements. Journal of Analytical Atomic Spectrometry 18, 1352-1356.

Georg, R.B., Reynolds, B.C., Frank, M., Halliday, A.N., 2006. Mechanisms controlling the silicon isotopic compositions of river waters. Earth and Planetary Science Letters 249, 290-306.

Godsey, S.E., Kirchner, J.W., Clow, D.W., 2009. Concentration-discharge relationships reflect chemostatic characteristics of US catchments. Hydrological Processes 23, 1844-1864.

Griffith, E.M., Schmitt, A.-D., Andrews, M.G., Fantle, M.S., 2020. Elucidating modern geochemical cycles at local, regional, and global scales using calcium isotopes. Chemical Geology 534.

Gurumurthy, G.P., Balakrishna, K., Tripti, M., Riotte, J., Audry, S., Braun, J.-J., Udaya Shankar, H.N., 2015. Use of Sr isotopes as a tool to decipher the soil weathering processes in a tropical river catchment, southwestern India. Applied Geochemistry 63, 498-506.

Hao, H., 2014. Breccia Mineralization and Geochemistry Studies of Duocaima Large Lead-Zinc Deposit in Tuotuohe Area. China University of Geosciences (Beijing).

He, Y., Wang, Y., Zhu, C., Huang, S., Li, S., 2017. Mass-Independent and Mass-Dependent Ca Isotopic Compositions of Thirteen Geological Reference Materials Measured by Thermal Ionisation Mass Spectrometry. Geostandards and Geoanalytical Research 41, 283-302.

Heuser, A., Eisenhauer, A., 2008. The Calcium Isotope Composition ($\delta^{44/40}$Ca) of NIST SRM 915b and NIST SRM 1486. Geostandards and Geoanalytical Research 32, 311-315.

Hindshaw, R.S., Reynolds, B.C., Wiederhold, J.G., Kretzschmar, R., Bourdon, B., 2011. Calcium isotopes in a proglacial weathering environment: Damma glacier, Switzerland. Geochimica et Cosmochimica Acta 75, 106-118.

Hindshaw, R.S., Teisserenc, R., Le Dantec, T., Tananaev, N., 2019. Seasonal change of geochemical sources and processes in the Yenisei River: A Sr, Mg and Li isotope study. Geochimica et Cosmochimica Acta 255, 222-236.

Hindshaw, R.S., Tosca, R., Tosca, N.J., Tipper, E.T., 2020. Experimental constraints on Mg isotope fractionation during clay formation: Implications for the global biogeochemical cycle of Mg. Earth and Planetary Science Letters 531, 115980.

Hippler, D., Schmitt, A.-D., Gussone, N., Heuser, A., Stille, P., Eisenhauer, A., Nägler, T.F., 2003. Calcium isotopic composition of various reference materials and seawater. geostandards and geoanalytical research 27, 13-19.

Holmden, C., Bélanger, N., 2010. Ca isotope cycling in a forested ecosystem. Geochimica et Cosmochimica Acta 74, 995-1015.

Huth, T.E., Cerling, T.E., Marchetti, D.W., Bowling, D.R., Ellwein, A.L., Passey, B.H., 2019. Seasonal

941 Bias in Soil Carbonate Formation and Its Implications for Interpreting High-Resolution
942 Paleoarchives: Evidence From Southern Utah. Journal of Geophysical Research:
943 Biogeosciences 124, 616-632.
944 Jacobson, A.D., Blum, J.D., 2000. Ca/Sr and $^{87}Sr/^{86}Sr$ geochemistry of disseminated calcite in Himalayan
945 silicate rocks from Nanga Parbat: Influence on river-water chemistry. Geology 28, 463-466.
946 Jacobson, A.D., Blum, J.D., Chamberlain, C.P., Poage, M.A., Sloan, V.F., 2002. Ca/Sr and Sr isotope
947 systematics of a Himalayan glacial chronosequence: Carbonate versus silicate weathering rates
948 as a function of landscape surface age. Geochimica et Cosmochimica Acta 66, 13-27.
949 Jacobson, A.D., Holmden, C., 2008. $\delta^{44}Ca$ evolution in a carbonate aquifer and its bearing on the
950 equilibrium isotope fractionation factor for calcite. Earth and Planetary Science Letters 270,
951 349-353.
952 Jacobson, A.D., Zhang, Z., Lundstrom, C., Huang, F., 2010. Behavior of Mg isotopes during
953 dedolomitization in the Madison Aquifer, South Dakota. Earth and Planetary Science Letters
954 297, 446-452.
955 Kajita, H., Ota, Y., Yoshimura, T., Araoka, D., Manaka, T., Ziyu, O., Iwasaki, S., Yanase, T., Inamura, A.,
956 Uchida, E., Zheng, H., Yang, Q., Wang, K., Suzuki, A., Kawahata, H., 2020. Seasonal and
957 Spatial Variations of Chemical Weathering in the Mekong Basin: From the Headwaters to the
958 Lower Reaches. Aquatic Geochemistry 26, 137-159.
959 Lehn, G.O., Jacobson, A.D., Douglas, T.A., McClelland, J.W., Barker, A.J., Khosh, M.S., 2017.
960 Constraining seasonal active layer dynamics and chemical weathering reactions occurring in
961 North Slope Alaskan watersheds with major ion and isotope ($\delta\ ^{34}S_{SO4}$, $\delta^{13}C_{DIC}$, $^{87}Sr/\ ^{86}Sr$,
962 $\delta^{44/40}Ca$, and $\delta^{44/42}Ca$) measurements. Geochimica et Cosmochimica Acta 217, 399-420.
963 Li, S.-L., Chetelat, B., Yue, F., Zhao, Z., Liu, C.-Q., 2014. Chemical weathering processes in the Yalong
964 River draining the eastern Tibetan Plateau, China. Journal of Asian Earth Sciences 88, 74-84.
965 Liu, F., Zhu, H.L., Li, X., Wang, G.Q., Zhang, Z.F., 2017. Calcium Isotopic Fractionation and
966 Compositions of Geochemical Reference Materials. Geostandards and Geoanalytical Research
967 41, 675-688.
968 Liu, X.-M., Teng, F.-Z., Rudnick, R.L., McDonough, W.F., Cummings, M.L., 2014. Massive magnesium
969 depletion and isotope fractionation in weathered basalts. Geochimica et Cosmochimica Acta
970 135, 336-349.
971 Lu, L., Wang, Q., Wang, G.-Q., Liu, Y.-L., Liu, C.-S., 2016. Trend of Climate Change over the Recent
972 60 Years and its Hydrological Responses for Jinsha River Basin. Journal of Noah China
973 University of Water Resources and Electric Power (Natural Science Edition) 37, 16-21 *(in*
974 *Chinese with English abstract)*.
975 Luo, C., Zheng, H., Tada, R., Wu, W., Irino, T., Yang, S., Saito, K., 2014. Tracing Sr isotopic composition
976 in space and time across the Yangtze River basin. Chemical Geology 388, 59-70.
977 Ma, J., Wei, G., Liu, Y., Ren, Z., Xu, Y., Yang, Y., 2013. Precise measurement of stable ($\delta^{88/86}Sr$) and
978 radiogenic ($^{87}Sr/^{86}Sr$) strontium isotope ratios in geological standard reference materials using
979 MC-ICP-MS. Chinese Science Bulletin 58, 3111-3118.
980 Ma, L., Teng, F.-Z., Jin, L., Ke, S., Yang, W., Gu, H.-O., Brantley, S.L., 2015. Magnesium isotope
981 fractionation during shale weathering in the Shale Hills Critical Zone Observatory:
982 Accumulation of light Mg isotopes in soils by clay mineral transformation. Chemical Geology
983 397, 37-50.
984 Ma, T., Weynell, M., Li, S.-L., Liu, Y., Chetelat, B., Zhong, J., Xu, S., Liu, C.-Q., 2020. Lithium isotope

compositions of the Yangtze River headwaters: weathering in high-relief catchments. Geochimica et Cosmochimica Acta 280, 46-65.

Maher, K., 2011. The role of fluid residence time and topographic scales in determining chemical fluxes from landscapes. Earth and Planetary Science Letters 312, 48-58.

Maher, K., Chamberlain, C.P., 2014. Hydrologic regulation of chemical weathering and the geologic carbon cycle. Science 343, 1502-1504.

Mavromatis, V., Gautier, Q., Bosc, O., Schott, J., 2013. Kinetics of Mg partition and Mg stable isotope fractionation during its incorporation in calcite. Geochimica et Cosmochimica Acta 114, 188-203.

Mavromatis, V., Prokushkin, A.S., Korets, M.A., Chmeleff, J., Mounic, S., Pokrovsky, O.S., 2020. Weak impact of landscape parameters and rock lithology on Mg isotope composition of the Yenisey River and its tributaries. Chemical Geology 540, 119547.

Meyer, N.A., Breecker, D.O., Young, M.H., Litvak, M.E., 2014. Simulating the Effect of Vegetation in Formation of Pedogenic Carbonate. Soil Science Society of America Journal 78, 914-924.

Michalopoulos, P., Aller, R.C., 1995. Rapid Clay Mineral Formation in Amazon Delta Sediments: Reverse Weathering and Oceanic Elemental Cycles. Science 270, 614-617.

Négrel, P., Petelet-Giraud, E., Guerrot, C., Millot, R., 2021. Ca and Sr isotope constraints on chemical weathering processes: A view through the Ebro river basin, Spain. Chemical Geology 578, 120324.

Nelson, C.J., Jacobson, A.D., Kitch, G.D., Weisenberger, T.B., 2021. Large calcium isotope fractionations by zeolite minerals from Iceland. Communications Earth & Environment 2, 206.

Nelson, C.J., Jacobson, A.D., Weisenberger, T.B., 2022. Controls on riverine calcium isotope ratios during basalt weathering in the Skagafjörður watershed, Iceland. Geochimica et Cosmochimica Acta 333, 216-241.

Noh, H., Huh, Y., Qin, J., Ellis, A., 2009. Chemical weathering in the Three Rivers region of Eastern Tibet. Geochimica et Cosmochimica Acta 73, 1857-1877.

Oelkers, E.H., Berninger, U.-N., Pérez-Fernàndez, A., Chmeleff, J., Mavromatis, V., 2018. The temporal evolution of magnesium isotope fractionation during hydromagnesite dissolution, precipitation, and at equilibrium. Geochimica et Cosmochimica Acta 226, 36-49.

Oelkers, E.H., Butcher, R., Pogge von Strandmann, P.A.E., Schuessler, J.A., von Blanckenburg, F., Snæbjörnsdóttir, S.Ó., Mesfin, K., Aradóttir, E.S., Gunnarsson, I., Sigfússon, B., Gunnlaugsson, E., Matter, J.M., Stute, M., Gislason, S.R., 2019. Using stable Mg isotope signatures to assess the fate of magnesium during the in situ mineralisation of CO_2 and H_2S at the CarbFix site in SW-Iceland. Geochimica et Cosmochimica Acta 245, 542-555.

Opfergelt, S., Burton, K.W., Georg, R.B., West, A.J., Guicharnaud, R.A., Sigfusson, B., Siebert, C., Gislason, S.R., Halliday, A.N., 2014. Magnesium retention on the soil exchange complex controlling Mg isotope variations in soils, soil solutions and vegetation in volcanic soils, Iceland. Geochimica et Cosmochimica Acta 125, 110-130.

Page, B.D., Bullen, T.D., Mitchell, M.J., 2008. Influences of calcium availability and tree species on Ca isotope fractionation in soil and vegetation. Biogeochemistry 88, 1-13.

Pearce, C.R., Saldi, G.D., Schott, J., Oelkers, E.H., 2012. Isotopic fractionation during congruent dissolution, precipitation and at equilibrium: Evidence from Mg isotopes. Geochimica et Cosmochimica Acta 92, 170-183.

Pett-Ridge, J.C., Derry, L.A., Kurtz, A.C., 2009. Sr isotopes as a tracer of weathering processes and dust

inputs in a tropical granitoid watershed, Luquillo Mountains, Puerto Rico. Geochimica et Cosmochimica Acta 73, 25-43.

Pogge von Strandmann, P.A.E., Burton, K.W., James, R.H., van Calsteren, P., Gislason, S.R., Sigfússon, B., 2008. The influence of weathering processes on riverine magnesium isotopes in a basaltic terrain. Earth and Planetary Science Letters 276, 187-197.

Pogge von Strandmann, P.A.E., Elliott, T., Marschall, H.R., Coath, C., Lai, Y.-J., Jeffcoate, A.B., Ionov, D.A., 2011. Variations of Li and Mg isotope ratios in bulk chondrites and mantle xenoliths. Geochimica Et Cosmochimica Acta 75, 5247-5268.

Pogge von Strandmann, P.A.E., Hendry, K.R., Hatton, J.E., Robinson, L.F., 2019a. The Response of Magnesium, Silicon, and Calcium Isotopes to Rapidly Uplifting and Weathering Terrains: South Island, New Zealand. Frontiers in Earth Science 7, 240.

Pogge von Strandmann, P.A.E., Olsson, J., Luu, T.-H., Gislason, S.R., Burton, K.W., 2019b. Using Mg Isotopes to Estimate Natural Calcite Compositions and Precipitation Rates During the 2010 Eyjafjallajökull Eruption. Frontiers in Earth Science 7, 6.

Rai, S.K., Singh, S.K., 2007. Temporal variation in Sr and $^{87}Sr/^{86}Sr$ of the Brahmaputra: Implications for annual fluxes and tracking flash floods through chemical and isotope composition. Geochemistry, Geophysics, Geosystems 8, Q08008.

Ren, F., Zhang, P., Chen, X., Xu, P., Chen, J., 2016. Vegetation Spatial Heterogeneity of Valleys along the Jinsha River and Its Influence on Ecological Restoration. Journal of Yangtze River Scientific Research Institute 33, 24-30 *(in Chinese with English Abstract)*.

Riebe, C.S., Kirchner, J.W., Finkel, R.C., 2004. Erosional and climatic effects on long-term chemical weathering rates in granitic landscapes spanning diverse climate regimes. Earth and Planetary Science Letters 224, 547-562.

Rutter, N., Hodson, A., Irvine-Fynn, T., Solås, M.K., 2011. Hydrology and hydrochemistry of a deglaciating high-Arctic catchment, Svalbard. Journal of Hydrology 410, 39-50.

Ryu, J.-S., Vigier, N., Decarreau, A., Lee, S.-W., Lee, K.-S., Song, H., Petit, S., 2016. Experimental investigation of Mg isotope fractionation during mineral dissolution and clay formation. Chemical Geology 445, 135-145.

Saulnier, S., Rollion-Bard, C., Vigier, N., Chaussidon, M., 2012. Mg isotope fractionation during calcite precipitation: An experimental study. Geochimica et Cosmochimica Acta 91, 75-91.

Schmitt, A.-D., Chabaux, F., Stille, P., 2003. The calcium riverine and hydrothermal isotopic fluxes and the oceanic calcium mass balance. Earth and Planetary Science Letters 213, 503-518.

Schott, J., Mavromatis, V., Fujii, T., Pearce, C.R., Oelkers, E.H., 2016. The control of carbonate mineral Mg isotope composition by aqueous speciation: Theoretical and experimental modeling. Chemical Geology 445, 120-134.

Stallard, R.F., Edmond, J.M., 1983. Geochemistry of the Amazon: 2. The influence of geology and weathering environment on the dissolved load. Journal of Geophysical Research: Oceans 88, 9671-9688.

Stewart, B.W., Capo, R.C., Chadwick, O.A., 1998. Quantitative strontium isotope models for weathering, pedogenesis and biogeochemical cycling. Geoderma 82, 173-195.

Sullivan, P.L., Ma, L., West, N., Jin, L., Karwan, D.L., Noireaux, J., Steinhoefel, G., Gaines, K.P., Eissenstat, D.M., Gaillardet, J., Derry, L.A., Meek, K., Hynek, S., Brantley, S.L., 2016. CZ-tope at Susquehanna Shale Hills CZO: Synthesizing multiple isotope proxies to elucidate Critical Zone processes across timescales in a temperate forested landscape. Chemical Geology 445,

103-119.
Sun, J., Zhu, X.K., Belshaw, N.S., Chen, W., Doroshkevich, A.G., Luo, W.J., Song, W.L., Chen, B.B., Cheng, Z.G., Li, Z.H., Wang, Y., Kynicky, J., Henderson, G.M., 2021. Ca isotope systematics of carbonatites: Insights into carbonatite source and evolution. Geochemical Perspectives Letters 17, 11-15.
Teng, F.-Z., 2017. Magnesium Isotope Geochemistry. Reviews in Mineralogy and Geochemistry 82, 219-287.
Tesoriero, A.J., Pankow, J.F., 1996. Solid solution partitioning of Sr^{2+}, Ba^{2+}, and Cd^{2+} to calcite. Geochimica et Cosmochimica Acta 60, 1053-1063.
Tipper, E., 2022. Magnesium Isotopes: Tracer for the Global Biogeochemical Cycle of Magnesium Past and Present or Archive of Alteration?
Tipper, E., Galy, A., Bickle, M., 2006a. Riverine evidence for a fractionated reservoir of Ca and Mg on the continents: Implications for the oceanic Ca cycle. Earth and Planetary Science Letters 247, 267-279.
Tipper, E., Galy, A., Gaillardet, J., Bickle, M., Elderfield, H., Carder, E., 2006b. The magnesium isotope budget of the modern ocean: Constraints from riverine magnesium isotope ratios. Earth and Planetary Science Letters 250, 241-253.
Tipper, E.T., Bickle, M.J., Galy, A., West, A.J., Pomiès, C., Chapman, H.J., 2006c. The short term climatic sensitivity of carbonate and silicate weathering fluxes: Insight from seasonal variations in river chemistry. Geochimica et Cosmochimica Acta 70, 2737-2754.
Tipper, E.T., Calmels, D., Gaillardet, J., Louvat, P., Capmas, F., Dubacq, B., 2012a. Positive correlation between Li and Mg isotope ratios in the river waters of the Mackenzie Basin challenges the interpretation of apparent isotopic fractionation during weathering. Earth and Planetary Science Letters 333-334, 35-45.
Tipper, E.T., Gaillardet, J., Galy, A., Louvat, P., Bickle, M.J., Capmas, F., 2010. Calcium isotope ratios in the world's largest rivers: A constraint on the maximum imbalance of oceanic calcium fluxes. Global Biogeochemical Cycles 24, GB3019.
Tipper, E.T., Galy, A., Bickle, M.J., 2008. Calcium and magnesium isotope systematics in rivers draining the Himalaya-Tibetan-Plateau region: Lithological or fractionation control? Geochimica et Cosmochimica Acta 72, 1057-1075.
Tipper, E.T., Lemarchand, E., Hindshaw, R.S., Reynolds, B.C., Bourdon, B., 2012b. Seasonal sensitivity of weathering processes: Hints from magnesium isotopes in a glacial stream. Chemical Geology 312, 80-92.
Tipper, E.T., Lemarchand, E., Hindshaw, R.S., Reynolds, B.C., Bourdon, B., 2012c. Seasonal sensitivity of weathering processes: Hints from magnesium isotopes in a glacial stream. Chemical Geology 312-313, 80-92.
Tipper, E.T., Stevenson, E.I., Alcock, V., Knight, A.C.G., Baronas, J.J., Hilton, R.G., Bickle, M.J., Larkin, C.S., Feng, L., Relph, K.E., Hughes, G., 2021. Global silicate weathering flux overestimated because of sediment–water cation exchange. Proceedings of the National Academy of Sciences 118, e2016430118.
Torres, M.A., West, A.J., Clark, K.E., 2015. Geomorphic regime modulates hydrologic control of chemical weathering in the Andes–Amazon. Geochimica et Cosmochimica Acta 166, 105-128.
Tripathy, G.R., Goswami, V., Singh, S.K., Chakrapani, G.J., 2010. Temporal variations in Sr and $^{87}Sr/^{86}Sr$ of the Ganga headwaters: estimates of dissolved Sr flux to the mainstream. Hydrological

Processes 24, 1159-1171.
Wang, T., Zhao, Y., Xu, C., Ciais, P., Liu, D., Yang, H., Piao, S., Yao, T., 2021. Atmospheric dynamic constraints on Tibetan Plateau freshwater under Paris climate targets. Nature Climate Change 11, 219-225.
Wang, W., Li, S.-L., Zhong, J., Slowinski, S., Li, S., Li, C., Su, J., Yi, Y., Dong, K., Xu, S., Van Cappellen, P., Liu, C.-Q., 2022. Carbonate mineral dissolution and photosynthesis-induced precipitation regulate inorganic carbon cycling along the karst river-reservoir continuum, SW China. Journal of Hydrology 615, 128621.
Wang, Y., Lei, X., Wen, X., Fang, G., Tan, Q., Tian, Y., Wang, C., Wang, H., 2019. Effects of damming and climatic change on the eco-hydrological system: A case study in the Yalong River, southwest China. Ecological Indicators 105, 663-674.
Wei, G., Ma, J., Liu, Y., Xie, L., Lu, W., Deng, W., Ren, Z., Zeng, T., Yang, Y., 2013. Seasonal changes in the radiogenic and stable strontium isotopic composition of Xijiang River water: Implications for chemical weathering. Chemical Geology 343, 67-75.
Weis, D., Kieffer, B., Maerschalk, C., Barling, J., de Jong, J., Williams, G.A., Hanano, D., Pretorius, W., Mattielli, N., Scoates, J.S., Goolaerts, A., Friedman, R.M., Mahoney, J.B., 2006. High-precision isotopic characterization of USGS reference materials by TIMS and MC-ICP-MS. Geochemistry, Geophysics, Geosystems 7, 1-30.
West, A., Galy, A., Bickle, M., 2005. Tectonic and climatic controls on silicate weathering. Earth and Planetary Science Letters 235, 211-228.
Wiegand, B.A., 2005. Ca cycling and isotopic fluxes in forested ecosystems in Hawaii. Geophysical Research Letters 32, 1-4.
Wimpenny, J., Burton, K.W., James, R.H., Gannoun, A., Mokadem, F., Gíslason, S.R., 2011. The behaviour of magnesium and its isotopes during glacial weathering in an ancient shield terrain in West Greenland. Earth and Planetary Science Letters 304, 260-269.
Wimpenny, J., Colla, C.A., Yin, Q.-Z., Rustad, J.R., Casey, W.H., 2014. Investigating the behaviour of Mg isotopes during the formation of clay minerals. Geochimica et Cosmochimica Acta 128, 178-194.
Wimpenny, J., Gíslason, S.R., James, R.H., Gannoun, A., Pogge Von Strandmann, P.A.E., Burton, K.W., 2010. The behaviour of Li and Mg isotopes during primary phase dissolution and secondary mineral formation in basalt. Geochimica et Cosmochimica Acta 74, 5259-5279.
Wu, W., Xu, S., Yang, J., Yin, H., 2008. Silicate weathering and CO_2 consumption deduced from the seven Chinese rivers originating in the Qinghai-Tibet Plateau. Chemical Geology 249, 307-320.
Wu, W., Yang, J., Xu, S., Li, G., Yin, H., Tao, X., 2009. Sr fluxes and isotopic compositions of the eleven rivers originating from the Qinghai-Tibet Plateau and their contributions to $^{87}Sr/^{86}Sr$ evolution of seawater. Science in China Series D: Earth Sciences 52, 1059-1067.
Xie, X., Li, H., Ju, Y., Chang, G., 2018. Analysis of Hydrological characteristics in Jinsha River Basin. Sichuan Water Resources 6, 101-104 *(in Chinese with English abstract).*
Xu, Y., Jin, Z., Gou, L.-F., Galy, A., Jin, C., Chen, C., Li, C., Deng, L., 2022. Carbonate weathering dominates magnesium isotopes in large rivers: Clues from the Yangtze River. Chemical Geology 588, 120677.
Yang, D., Yang, H., Lei, H., 2014. Watershed Hydrology. Tsinghua University Press.
Ye, R., Chang, J., 2019. Study of groundwater in permafrost regions of China: status and process. Journal of Glaciology and Geocryology 41, 183-196.

Young, E.D., Galy, A., 2004. The Isotope Geochemistry and Cosmochemistry of Magnesium. Reviews in Mineralogy and Geochemistry 55, 197-230.

Zhang, X., Xu, Z., Liu, W., Moon, S., Zhao, T., Zhou, X., Zhang, J., Wu, Y., Jiang, H., Zhou, L., 2019. Hydro-Geochemical and Sr Isotope Characteristics of the Yalong River Basin, Eastern Tibetan Plateau: Implications for Chemical Weathering and Controlling Factors. Geochemistry, Geophysics, Geosystems 20, 1221-1239.

Zhao, J.-C., Geng, D.-Q., Peng, J.-H., Liu, C.-Q., J.Gaillardet, Li, W.-P., He, Q.-C., 2003. Origin of major elements and Sr isotope for river water in Yangtze River source area. Hydrogeology & Engineering Geology, 89-93 *(in Chinese with English abstract)*.

Zhao, T., Liu, W., Xu, Z., Sun, H., Zhou, X., Zhou, L., Zhang, J., Zhang, X., Jiang, H., Liu, T., 2019. The influence of carbonate precipitation on riverine magnesium isotope signals: new constrains from Jinsha River Basin, Southeast Tibetan Plateau. Geochimica et Cosmochimica Acta 248, 172-184.

Zhong, J., 2017. Chemical weathering and carbon biogeochemical processes in the upper Changjiang Basin impacted by the hydrological conditions, Institute of Geochemistry, Chinese Academy of Sciences. The University of Chinese Academy of Sciences (*in Chinese with English abstract*).

Zhong, J., Li, S.-L., Zhu, X., Liu, J., Xu, S., Xu, S., Liu, C.-Q., 2021. Dynamics and fluxes of dissolved carbon under short-term climate variabilities in headwaters of the Changjiang River, draining the Qinghai-Tibet Plateau. Journal of Hydrology 596, 126128.

Zhu, D., 2007. China Water System Dictionary, (second edition). Qingdao Press (in Chinese). Qingdao.

Zhu, P., Macdougall, J.D., 1988. Calcium isotopes in the marine environment and the oceanic calcium cycle. Geochim Cosmochim Acta 62, 1691-1698.

Zieliński, M., Dopieralska, J., Belka, Z., Walczak, A., Siepak, M., Jakubowicz, M., 2018. Strontium isotope identification of water mixing and recharge sources in a river system (Oder River, central Europe): A quantitative approach. Hydrological Processes 32, 2597-2611.

Figure captions

Fig. 1. Setting and characteristics of the upper reaches of the Changjiang River. (a) Geological map with locations of the river water sampling stations marked by red stars (modified from (Chen et al., 2020)). (b) Permafrost distribution (modified from (Zhong et al., 2021)). (c) Air temperature (red line) and daily precipitation (blue bars) for the Yalong and Jinsha rivers from November 2013 to October 2014 (based on data from Panzhihua station).

Fig. 2. Seasonal variations of discharge (blue shading) and elemental concentrations (Ca, Mg, Na, K, Sr, Al, Fe, F, Cl, SO_4) (coloured lines) calculated by LOADEST for (a,c) the Jinsha River and (b,d) the Yalong River. The purple bar in (a,c) represents the initial permafrost thaw season for the Jinsha River. The grey bar in (b,d) represents the initial snow melt season for the Yalong River.

Fig. 3. Relationships between (a-d) selected elemental concentrations (Si, Sr, Ca, and Mg), (e) Si/Ca ratio, (f-h) isotopic compositions (Sr, Ca, Mg), and discharge during one hydrological year. In panels (a-d), the red and blue solid curves correspond to theoretical dilution lines for ion concentrations of the Jinsha and Yalong River, respectively. The vertical grey dashed lines represent discharge values of 2000 m^3/s and 4000 m^3/s, used to separate the low, medium, and high runoff regimes.

Fig. 4. Seasonal changes in Si/Ca, $^{87}Sr/^{86}Sr$, $\delta^{44/40}Ca$, and $\delta^{26}Mg$ values, and discharge in (a) the Jinsha River and (b) the Yalong River. The purple shaded bar in (a) represents the initial thawing of permafrost. The yellow shaded bar in (b) represents the initial melting of glaciers and snow. The blue shaded bar in both panels represents the wet season. The red and grey symbols for the Sr isotope data in panel (a) represent measured values and values corrected for evaporite input, respectively. Error bars for Ca and Mg isotope data are shown in panel (a) and represent the external 2sd. For Sr isotope data, the 2sd on $^{87}Sr/^{86}Sr$ values is 0.00002, which is smaller than the symbol sizes.

Fig. 5. (a, b) Seasonal variations in carbonate (ω_carb), silicate (ω_sil), and evaporite (ω_eva) weathering proportions in (a) the Jinsha River and (b) the Yalong River. Discharge is also shown and the blue shaded bar in both panels represents the wet season.

Fig. 6. Geochemical cross plots for Sr isotopes in the Jinsha and Yalong rivers. (a) $^{87}Sr/^{86}Sr$ versus Ca/Sr. (c) $^{87}Sr/^{86}Sr$ versus Na/Sr. Panels (b) and (d) correspond to panels (a) and (c), but with samples separated according to the low, medium, and high runoff periods. The grey shaded area represents the mixing field between the main sources, including meltwater, evaporites, and soil solutions (inferred from leachates) (Table 2). In the legend, JS and YL represent the time series samples from the Jinsha and Yalong rivers, respectively, while samples divided as 'High', 'Medium', and 'Low' are the time series samples collected during the high, medium, and low runoff periods. Data from the tributaries of the two rivers are also plotted (Chen et al., 2020; Chen et al., 2022).

Fig. 7. Geochemical cross plots for Ca isotopes in the Jinsha and Yalong rivers. (a) $\delta^{44/40}Ca$ versus $^{87}Sr/^{86}Sr$; (b) $\delta^{44/40}Ca$ versus SO_4/Ca; (c) $\delta^{44/40}Ca$ versus Sr/Ca; (d) $\delta^{44/40}Ca$ versus water temperature (T). In panels (a-c), the grey shaded area represents the mixing field between meltwater, evaporites, and soil solutions (inferred from leachates). The red dashed lines represent best-fit lines for the Jinsha time series samples during the low runoff season. Symbols, abbreviations, and data sources are as in Figure 6.

Fig. 8. Geochemical cross plots for Mg isotopes in the Jinsha and Yalong rivers. (a) $\delta^{26}Mg$ versus $^{87}Sr/^{86}Sr$; (b) $\delta^{26}Mg$ versus $\delta^{44/40}Ca$; (c) $\delta^{26}Mg$ versus illite saturation index (ISI); (d) $\delta^{26}Mg$ versus dolomite saturation index (DSI). Symbols, abbreviations, and data sources are as in Figure 6. In panel (c), the blue dashed line is the best-fit line for the low runoff seasons of the Yalong river waters.

Fig. 9. Schematic illustration of water sources and flow paths for the Jinsha and Yalong river basins during (a,b) the dry season with low runoff (Q<2000m3/s), (c,d) the intermediate runoff period (2000m3/s<Q<4000m3/s), and (e,f) the wet season with high runoff (Q>4000m3/s).

Tables

Table 1. Water chemistry and Sr, Ca, and Mg isotope data for the Jinsha and Yalong rivers at fixed sampling sites.

Table 2. Chemistry and Sr, Ca, and Mg isotope data from soil and river bedload (bulk and leachates) and bedrock from the upper reaches of the Changjiang River basin.

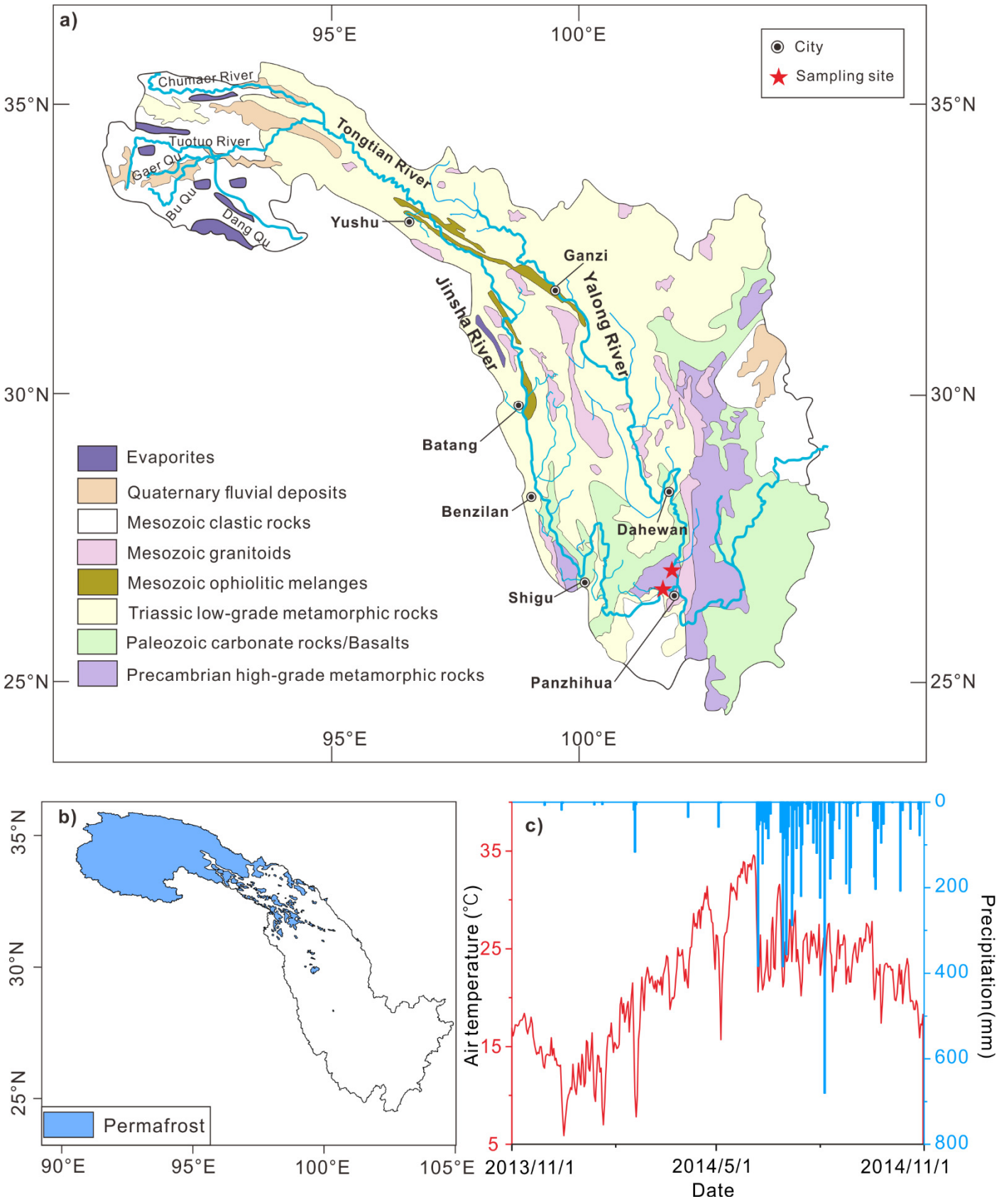
a)
95°E
100°E
35°N
30°N
25°N
City
Sampling site
Chumaer River
Tuotuo River
Gaer Qu
Bu Qu
Dang Qu
Tongtian River
Yushu
Ganzi
Yalong River
Jinsha River
Batang
Benzilan
Dahewan
Shigu
Panzhihua
Evaporites
Quaternary fluvial deposits
Mesozoic clastic rocks
Mesozoic granitoids
Mesozoic ophiolitic melanges
Triassic low-grade metamorphic rocks
Paleozoic carbonate rocks/Basalts
Precambrian high-grade metamorphic rocks
b)
Permafrost
90°E
95°E
100°E
105°E
c)
Air temperature (°C)
Precipitation(mm)
2013/11/1
2014/5/1
2014/11/1
Date

Fig. 1.

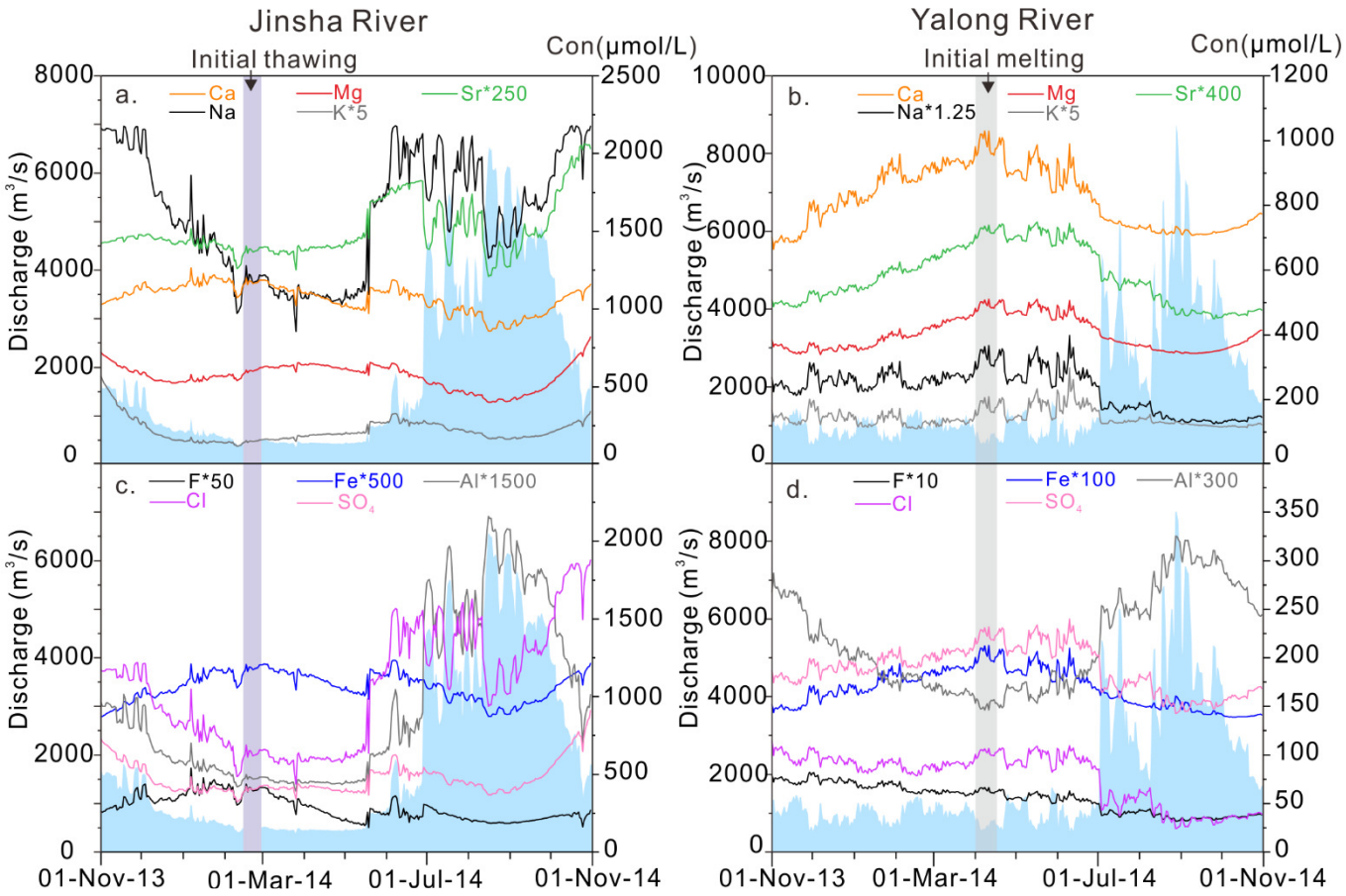
Jinsha River
Initial thawing
Con(μmol/L)
a.
Ca
Na
Mg
K*5
Sr*250
Discharge (m3/s)
c.
F*50
Cl
Fe*500
SO4
Al*1500
Yalong River
Initial melting
b.
Ca
Na*1.25
Mg
K*5
Sr*400
d.
F*10
Cl
Fe*100
SO4
Al*300
01-Nov-13
01-Mar-14
01-Jul-14
01-Nov-14

Fig. 2.

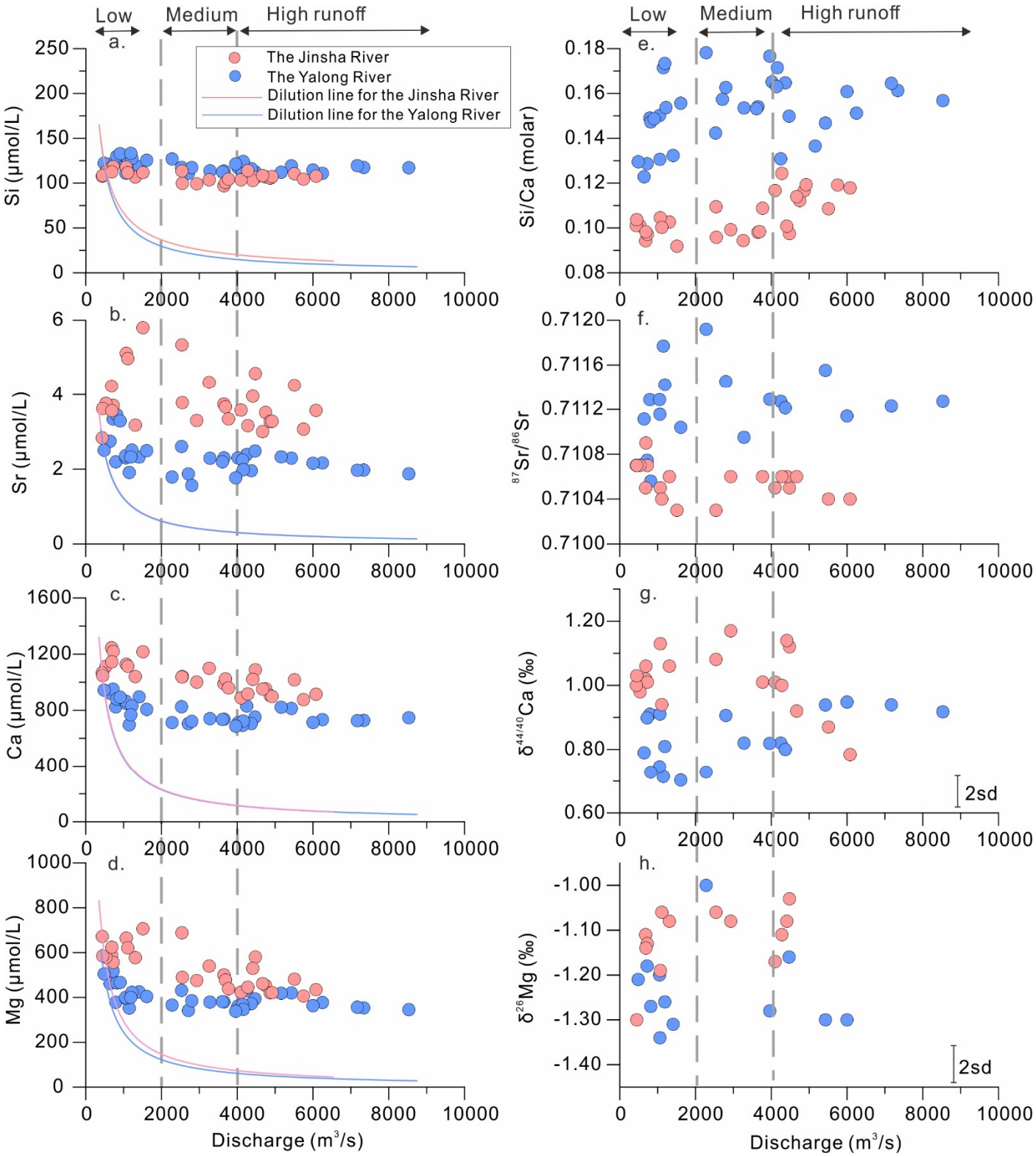
Low
Medium
High runoff
a.
The Jinsha River
The Yalong River
Dilution line for the Jinsha River
Dilution line for the Yalong River
Si (μmol/L)
b.
Sr (μmol/L)
c.
Ca (μmol/L)
d.
Mg (μmol/L)
Discharge (m3/s)
e.
Si/Ca (molar)
f.
87Sr/86Sr
g.
δ44/40Ca (‰)
2sd
h.
δ26Mg (‰)
2sd
Discharge (m3/s)

Fig. 3.

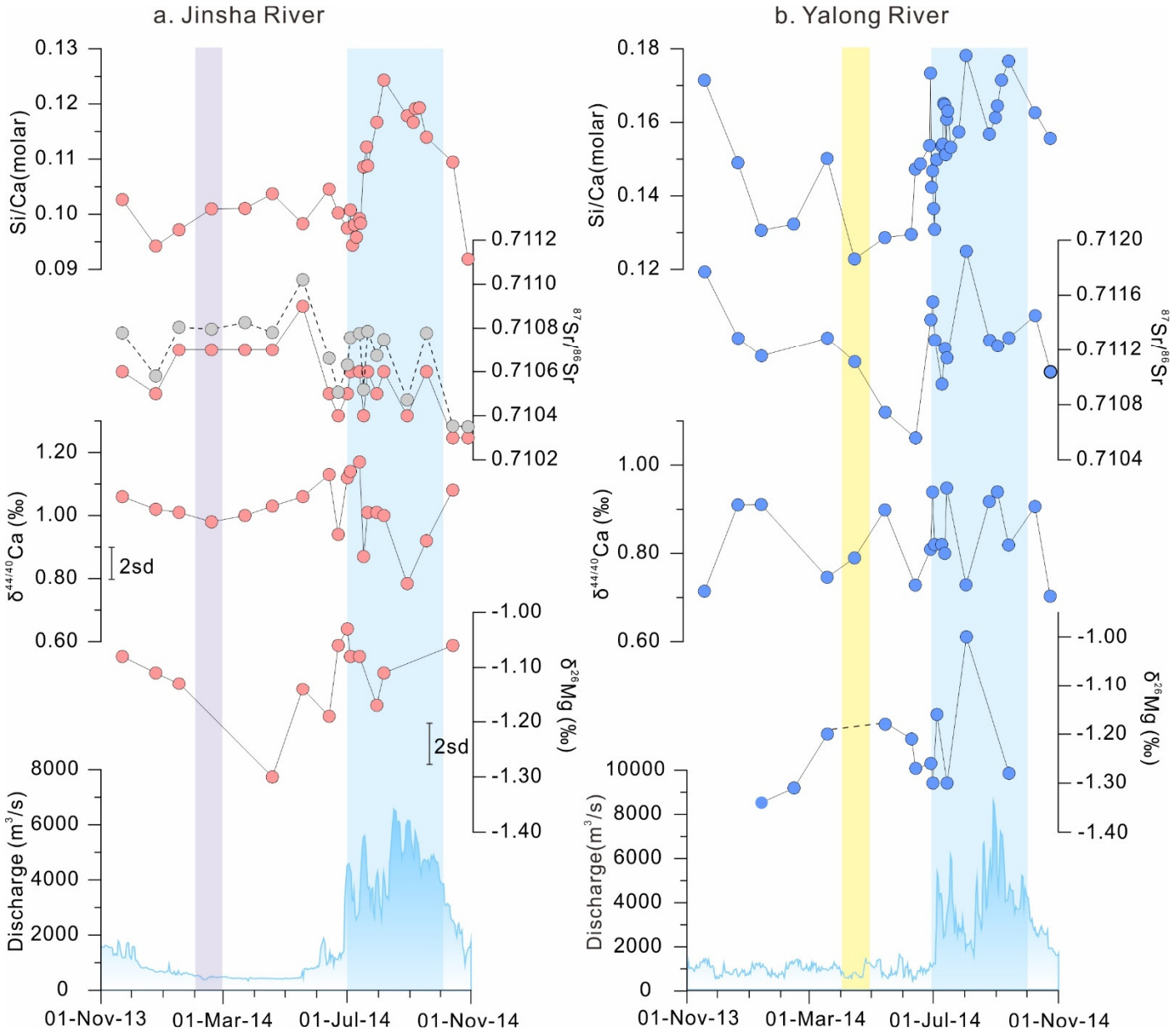
a. Jinsha River
b. Yalong River
Si/Ca(molar)
$^{87}Sr/^{86}Sr$
$\delta^{44/40}Ca$ (‰)
$\delta^{26}Mg$ (‰)
Discharge (m^3/s)
2sd
01-Nov-13
01-Mar-14
01-Jul-14
01-Nov-14

Fig. 4.

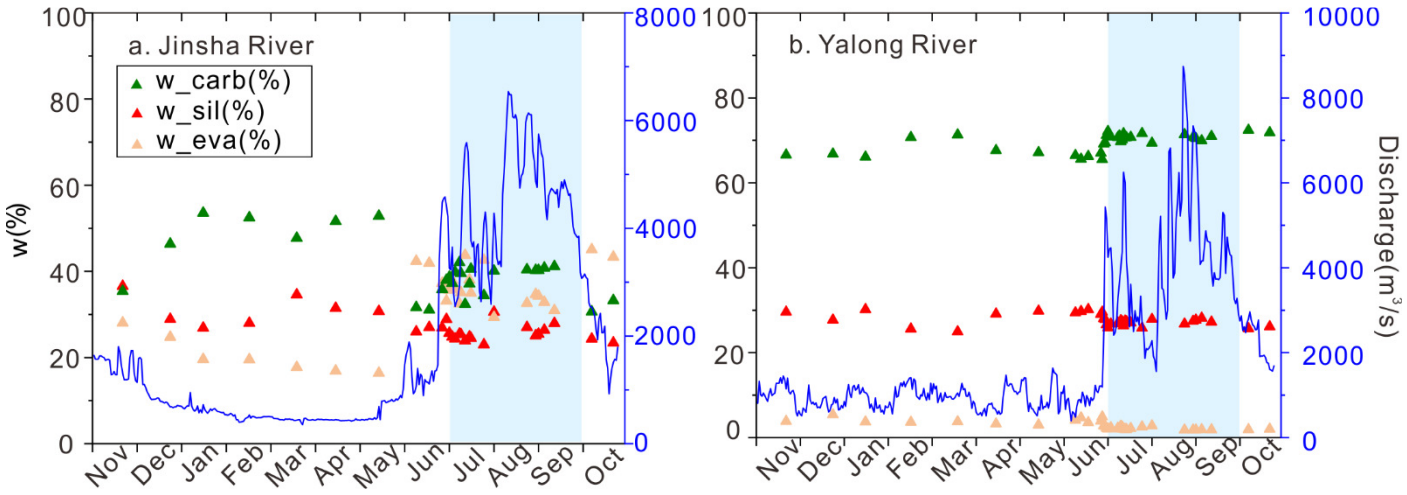
a. Jinsha River
w_carb(%)
w_sil(%)
w_eva(%)
w(%)
Discharge(m3/s)
b. Yalong River
Nov
Dec
Jan
Feb
Mar
Apr
May
Jun
Jul
Aug
Sep
Oct

Fig. 5.

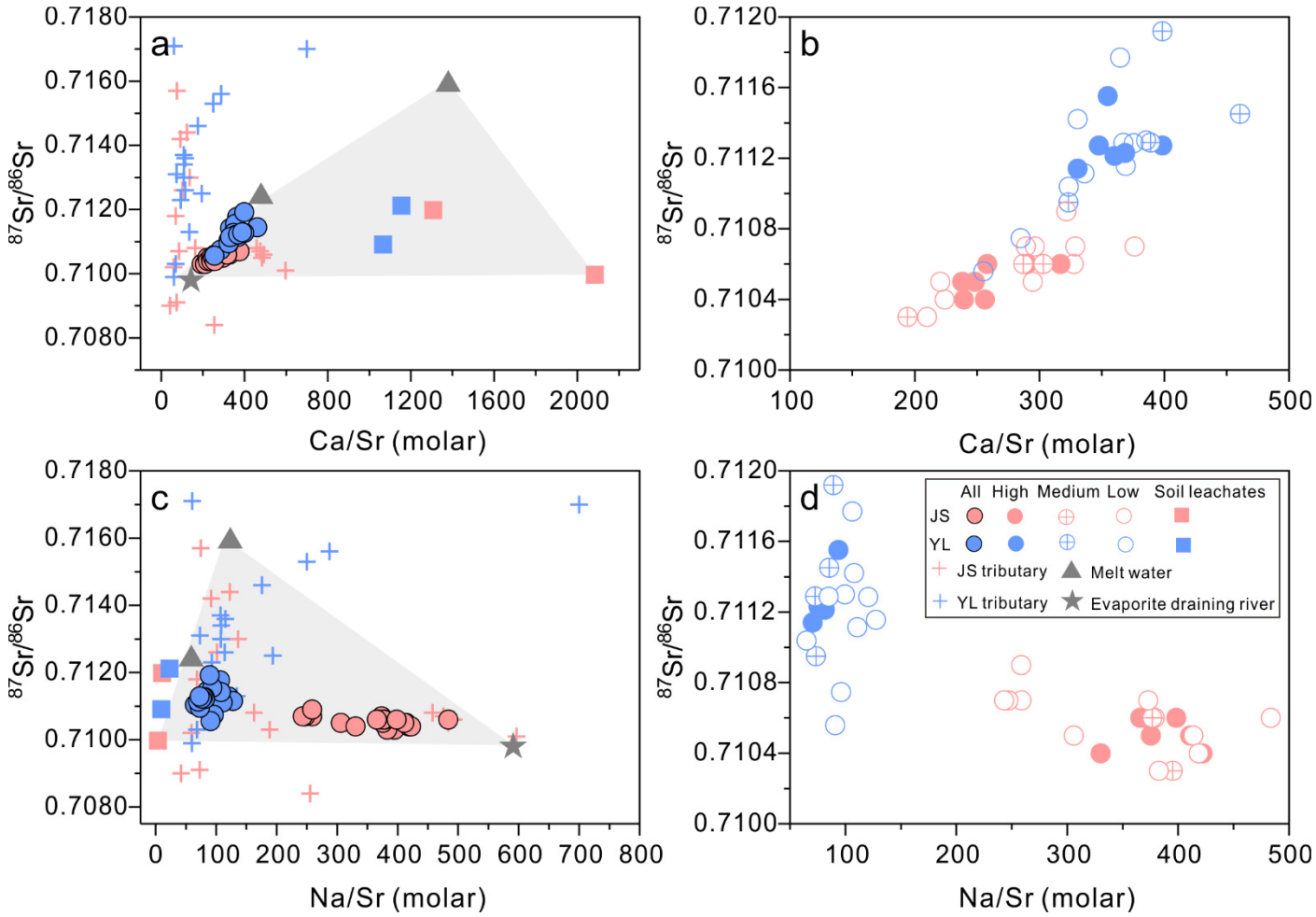
a
b
c
d
$^{87}Sr/^{86}Sr$
Ca/Sr (molar)
Na/Sr (molar)
All
High
Medium
Low
Soil leachates
JS
YL
JS tributary
YL tributary
Melt water
Evaporite draining river

Fig. 6.

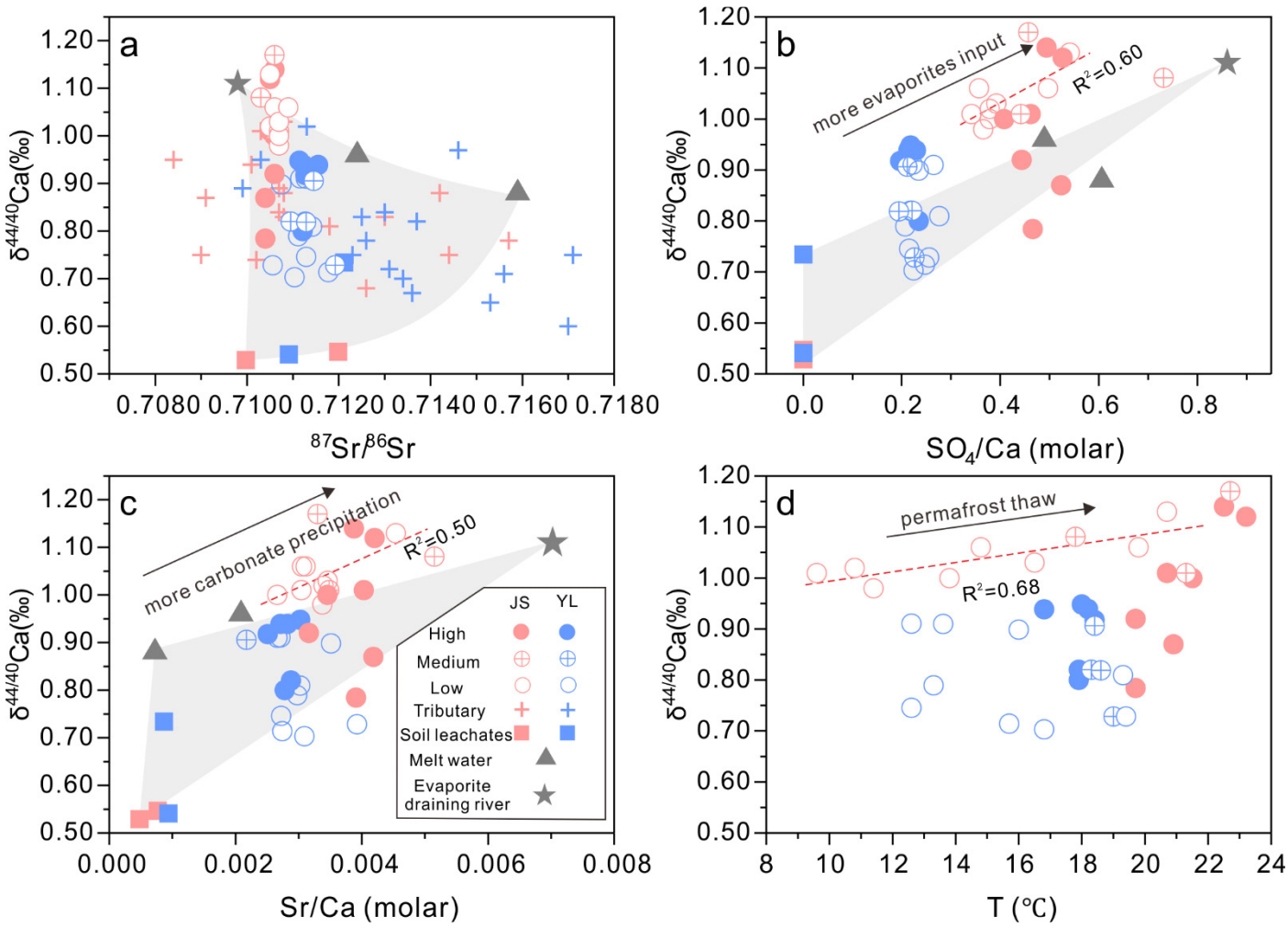
a
b
c
d
δ44/40Ca(‰)
87Sr/86Sr
SO4/Ca (molar)
Sr/Ca (molar)
T (℃)
more evaporites input
R²=0.60
more carbonate precipitation
R²=0.50
permafrost thaw
R²=0.68
JS
YL
High
Medium
Low
Tributary
Soil leachates
Melt water
Evaporite draining river

Fig. 7.

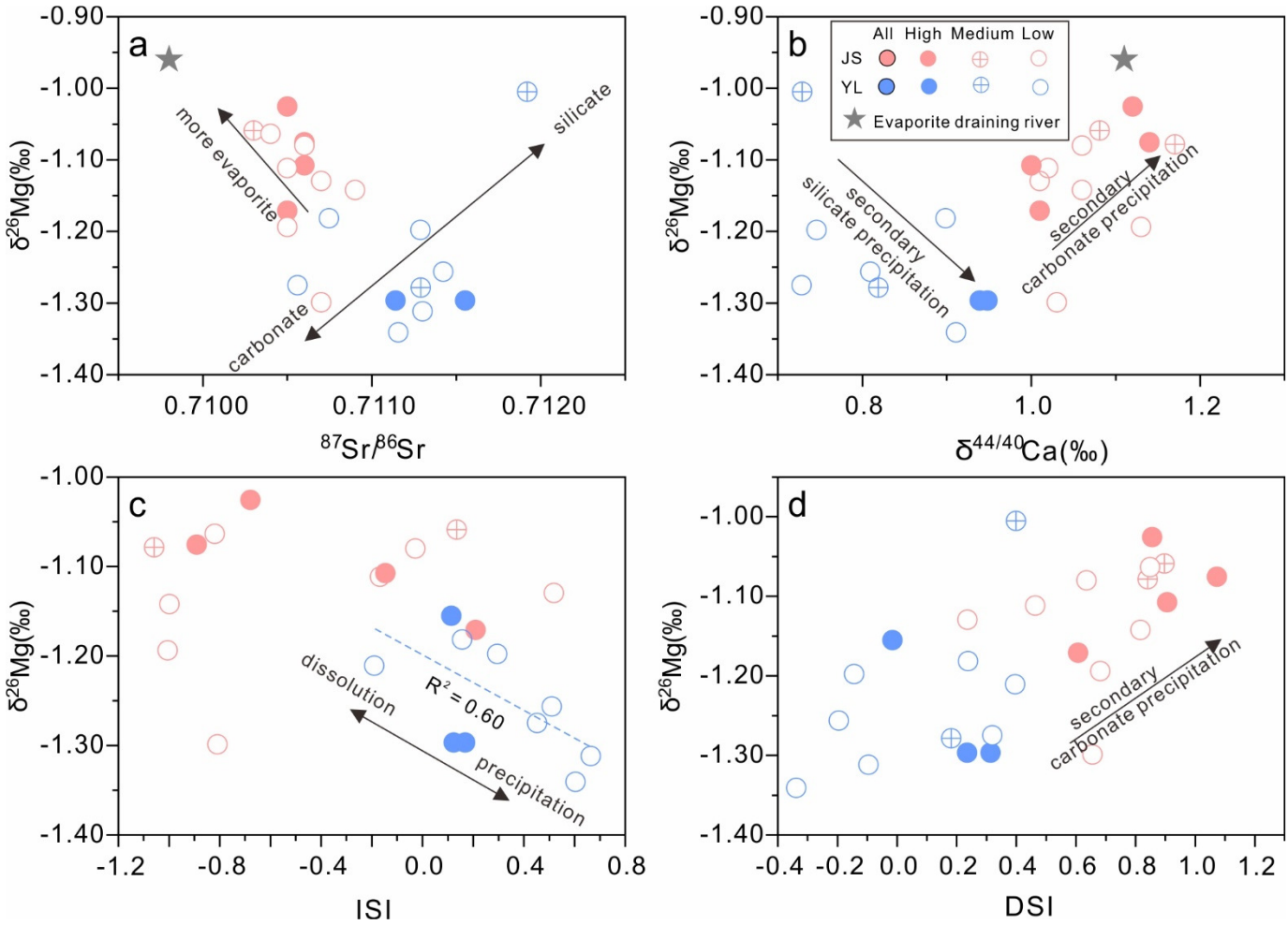
a
b
c
d
δ26Mg(‰)
87Sr/86Sr
δ44/40Ca(‰)
ISI
DSI
more evaporite
silicate
carbonate
All High Medium Low
JS
YL
Evaporite draining river
secondary silicate precipitation
secondary carbonate precipitation
dissolution
precipitation
R2 = 0.60

Fig. 8.

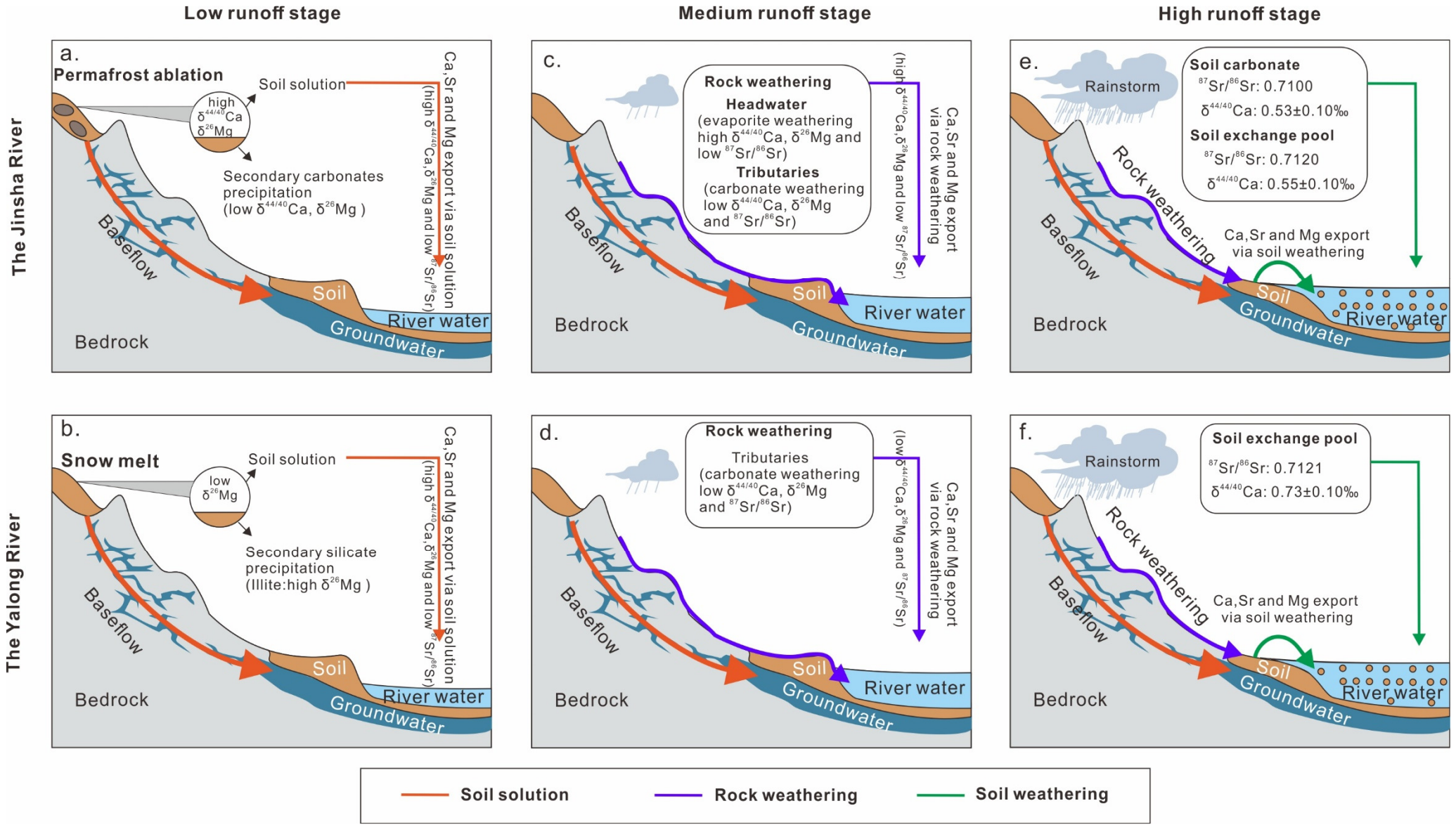
Low runoff stage
Medium runoff stage
High runoff stage
The Jinsha River
The Yalong River
a.
Permafrost ablation
Soil solution
high δ44/40Ca δ26Mg
Secondary carbonates precipitation (low δ44/40Ca, δ26Mg)
Ca,Sr and Mg export via soil solution (high δ44/40Ca,δ26Mg and low 87Sr/86Sr)
Baseflow
Soil
River water
Groundwater
Bedrock
b.
Snow melt
Soil solution
low δ26Mg
Secondary silicate precipitation (Illite:high δ26Mg)
Ca,Sr and Mg export via soil solution (high δ44/40Ca,δ26Mg and low 87Sr/86Sr)
Baseflow
Soil
River water
Groundwater
Bedrock
c.
Rock weathering
Headwater
(evaporite weathering high δ44/40Ca, δ26Mg and low 87Sr/86Sr)
Tributaries
(carbonate weathering low δ44/40Ca, δ26Mg and 87Sr/86Sr)
(high δ44/40Ca,δ26Mg and low 87Sr/86Sr)
Ca,Sr and Mg export via rock weathering
Baseflow
Soil
River water
Groundwater
Bedrock
d.
Rock weathering
Tributaries
(carbonate weathering low δ44/40Ca, δ26Mg and 87Sr/86Sr)
(low δ44/40Ca,δ26Mg and 87Sr/86Sr)
Ca,Sr and Mg export via rock weathering
Baseflow
Soil
River water
Groundwater
Bedrock
e.
Rainstorm
Soil carbonate
87Sr/86Sr: 0.7100
δ44/40Ca: 0.53±0.10‰
Soil exchange pool
87Sr/86Sr: 0.7120
δ44/40Ca: 0.55±0.10‰
Rock weathering
Ca,Sr and Mg export via soil weathering
Baseflow
Soil
River water
Groundwater
Bedrock
f.
Rainstorm
Soil exchange pool
87Sr/86Sr: 0.7121
δ44/40Ca: 0.73±0.10‰
Rock weathering
Ca,Sr and Mg export via soil weathering
Baseflow
Soil
River water
Groundwater
Bedrock
Soil solution
Rock weathering
Soil weathering

Fig. 9.

Supplementary information for

Behaviour of Sr, Ca, and Mg isotopes under variable hydrological conditions in high-relief large river systems

Bei-Bei Chen [a, b], Si-Liang Li [b, c *], Philip A.E. Pogge von Strandmann [d, e], David J. Wilson [d], Jun Zhong [b], Ting-Ting Ma [b], Jian Sun [f], Cong-Qiang Liu [b]

a State Key Laboratory of Geological Processes and Mineral Resources, China University of Geosciences, Beijing

b Institute of Surface-Earth System Science, School of Earth System Science, Tianjin University, Tianjin 300072, China

c State Key Laboratory of Hydraulic Engineering Simulation and Safety, Tianjin University, Tianjin 300072, China

d London Geochemistry and Isotope Centre (LOGIC), Institute of Earth and Planetary Sciences, University College London and Birkbeck, University of London, Gower Street, London WC1E 6BT, UK

e Mainz Isotopes and Geochemistry (MIGHTY), Institute of Geosciences, Johannes Gutenberg University, 55122 Mainz, Germany

f Key Laboratory of Deep-Earth Dynamics of Ministry of Natural Resources, MNR Key Laboratory of Isotope Geology, Institute of Geology, Chinese Academy of Geological Sciences, Beijing 100037, China

Figure S1-S4:

Fig. S1. Magnesium three-isotope diagram for samples analysed in this study. Note that all samples fall on a single mass-dependent fractionation line.

Fig. S2. The forward model used to calculate the contribution of different endmembers to the river waters (modified from (Noh et al., 2009)). The detailed endmember values for all elements can be found in Table 2.

Fig. S3. Relationships between discharge and a range of chemical weathering parameters in the Jinsha and Yalong rivers. CWR, SWR, and EWR represent the weathering rates of carbonates, silicates, and evaporites, respectively. TCWR represents total chemical weathering rates, and E represents erosion rates. The parameters w_carb, w_sil, and w_eva represent the proportions of carbonate, silicate, and evaporite weathering to total chemical weathering.

Fig. S4. Relationships of (a) dolomite saturation index (DSI), (b) calcite saturation index (CSI), and (c) illite saturation index (ISI) with discharge in the Jinsha (JS) and Yalong (YL) rivers. (d) Relationship between $\delta^{26}Mg$ values and SO_4/Mg ratios.

Tables S1-S8:

Table S1. Typical operating parameters for stable Ca isotope ratio measurement using Nu Plasma HR MC-ICPMS.

Table S2. Stable Ca isotopic composition of geological reference materials from this study.

Table S3. $^{87}Sr/^{86}Sr$ values of geological reference materials from this study.

Table S4. LOADEST program settings used for concentration and flux calculations.

Table S5. Monthly average discharge and suspended particulate matter content in the Jinsha and Yalong rivers.

Table S6. Contribution of different endmembers to river water chemistry.

Table S7. Seasonal variations in chemical weathering rates and proportions (w) for different lithologies.

Table S8. Mineral saturation indices calculated for Jinsha and Yalong river waters.

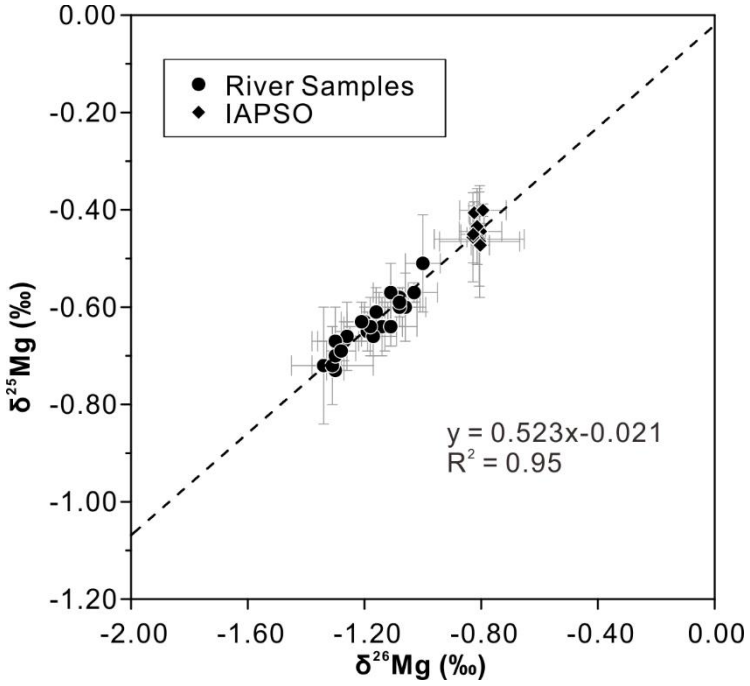
River Samples
IAPSO
y = 0.523x-0.021
R2 = 0.95
δ25Mg (‰)
δ26Mg (‰)
0.00
-0.20
-0.40
-0.60
-0.80
-1.00
-1.20
-2.00
-1.60
-1.20
-0.80
-0.40
0.00

Fig. S1

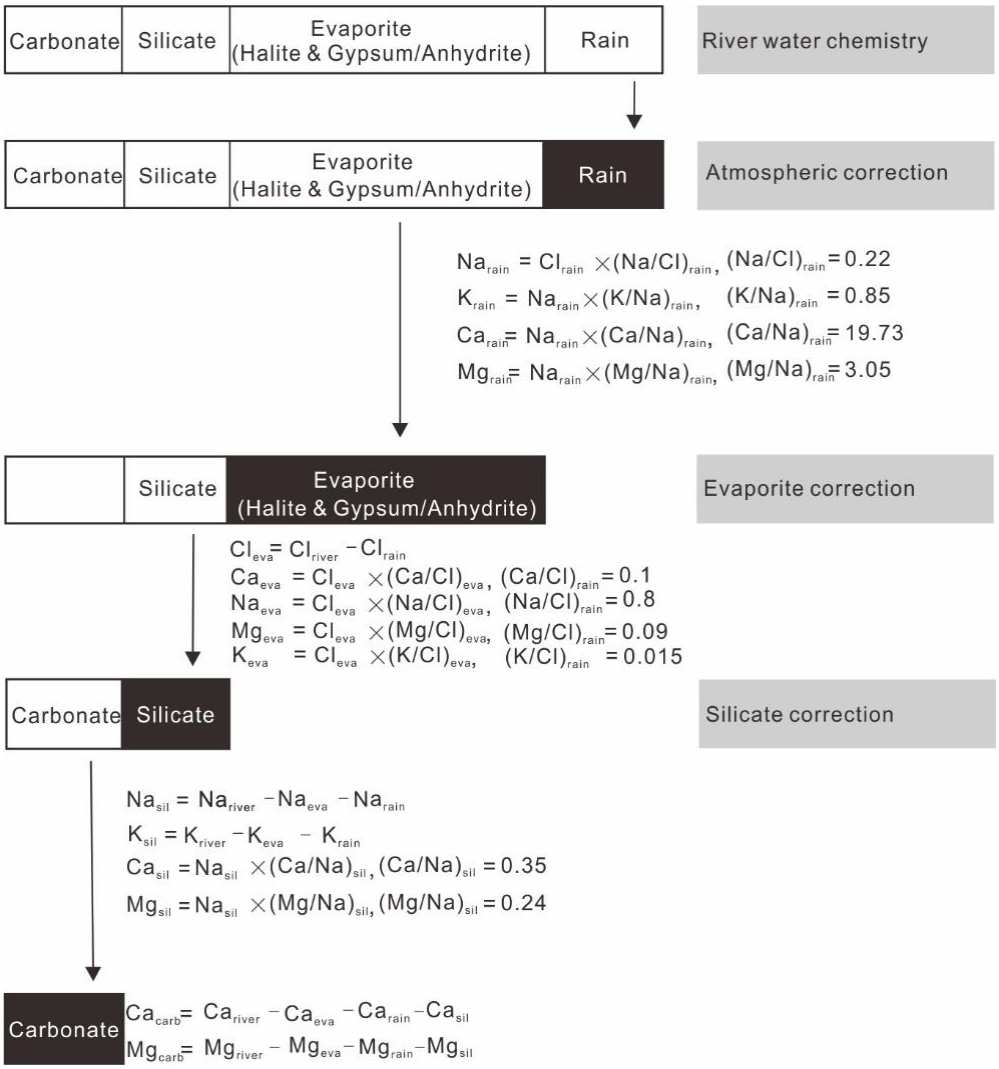
Carbonate
Silicate
Evaporite (Halite & Gypsum/Anhydrite)
Rain
River water chemistry
Atmospheric correction
$Na_{rain} = Cl_{rain} \times (Na/Cl)_{rain}$, $(Na/Cl)_{rain} = 0.22$
$K_{rain} = Na_{rain} \times (K/Na)_{rain}$, $(K/Na)_{rain} = 0.85$
$Ca_{rain} = Na_{rain} \times (Ca/Na)_{rain}$, $(Ca/Na)_{rain} = 19.73$
$Mg_{rain} = Na_{rain} \times (Mg/Na)_{rain}$, $(Mg/Na)_{rain} = 3.05$
Evaporite correction
$Cl_{eva} = Cl_{river} - Cl_{rain}$
$Ca_{eva} = Cl_{eva} \times (Ca/Cl)_{eva}$, $(Ca/Cl)_{rain} = 0.1$
$Na_{eva} = Cl_{eva} \times (Na/Cl)_{eva}$, $(Na/Cl)_{rain} = 0.8$
$Mg_{eva} = Cl_{eva} \times (Mg/Cl)_{eva}$, $(Mg/Cl)_{rain} = 0.09$
$K_{eva} = Cl_{eva} \times (K/Cl)_{eva}$, $(K/Cl)_{rain} = 0.015$
Silicate correction
$Na_{sil} = Na_{river} - Na_{eva} - Na_{rain}$
$K_{sil} = K_{river} - K_{eva} - K_{rain}$
$Ca_{sil} = Na_{sil} \times (Ca/Na)_{sil}$, $(Ca/Na)_{sil} = 0.35$
$Mg_{sil} = Na_{sil} \times (Mg/Na)_{sil}$, $(Mg/Na)_{sil} = 0.24$
$Ca_{carb} = Ca_{river} - Ca_{eva} - Ca_{rain} - Ca_{sil}$
$Mg_{carb} = Mg_{river} - Mg_{eva} - Mg_{rain} - Mg_{sil}$

Fig. S2

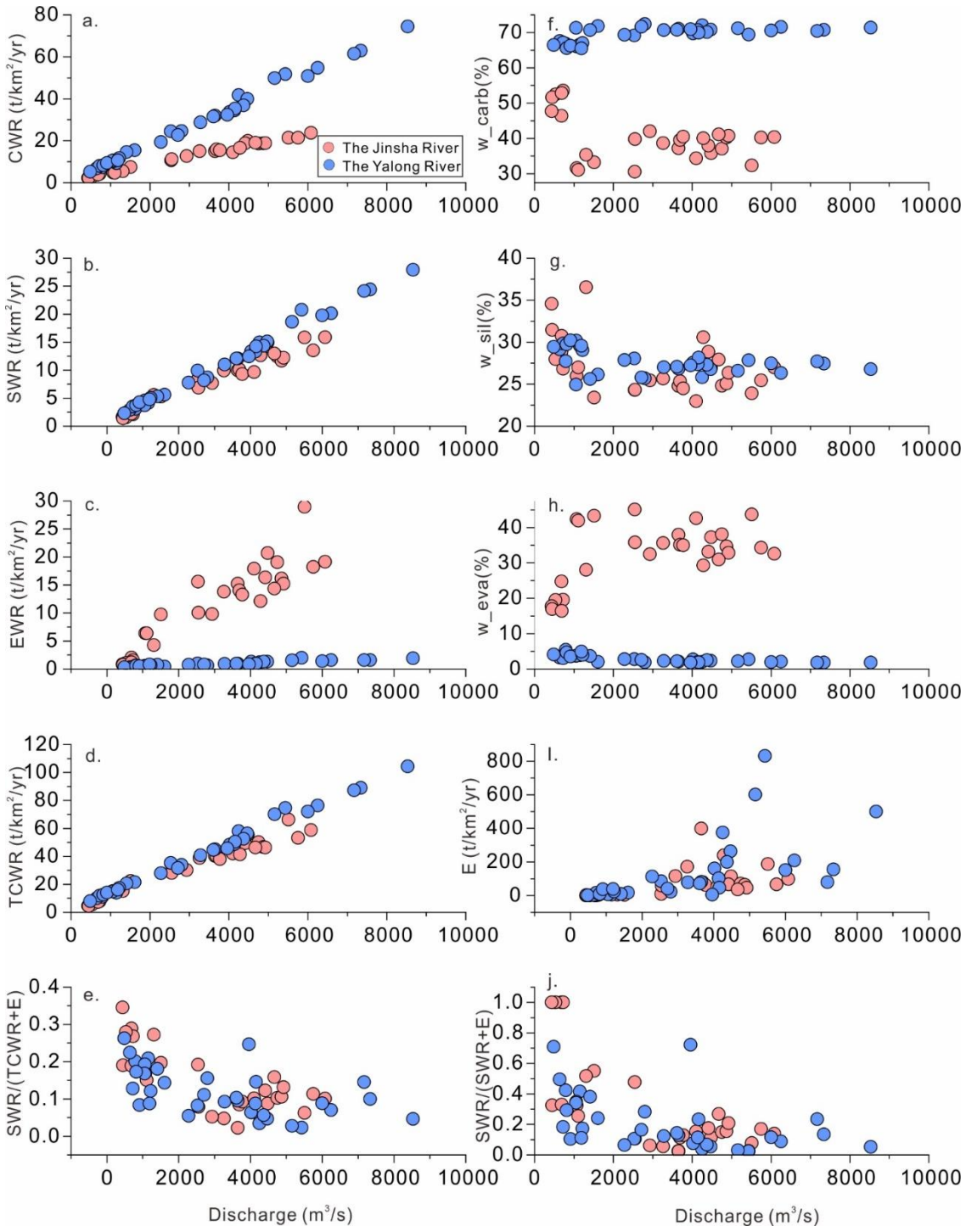
a.
CWR (t/km²/yr)
The Jinsha River
The Yalong River
b.
SWR (t/km²/yr)
c.
EWR (t/km²/yr)
d.
TCWR (t/km²/yr)
e.
SWR/(TCWR+E)
f.
w_carb(%)
g.
w_sil(%)
h.
w_eva(%)
I.
E (t/km²/yr)
j.
SWR/(SWR+E)
Discharge (m³/s)
Discharge (m³/s)

Fig. S3

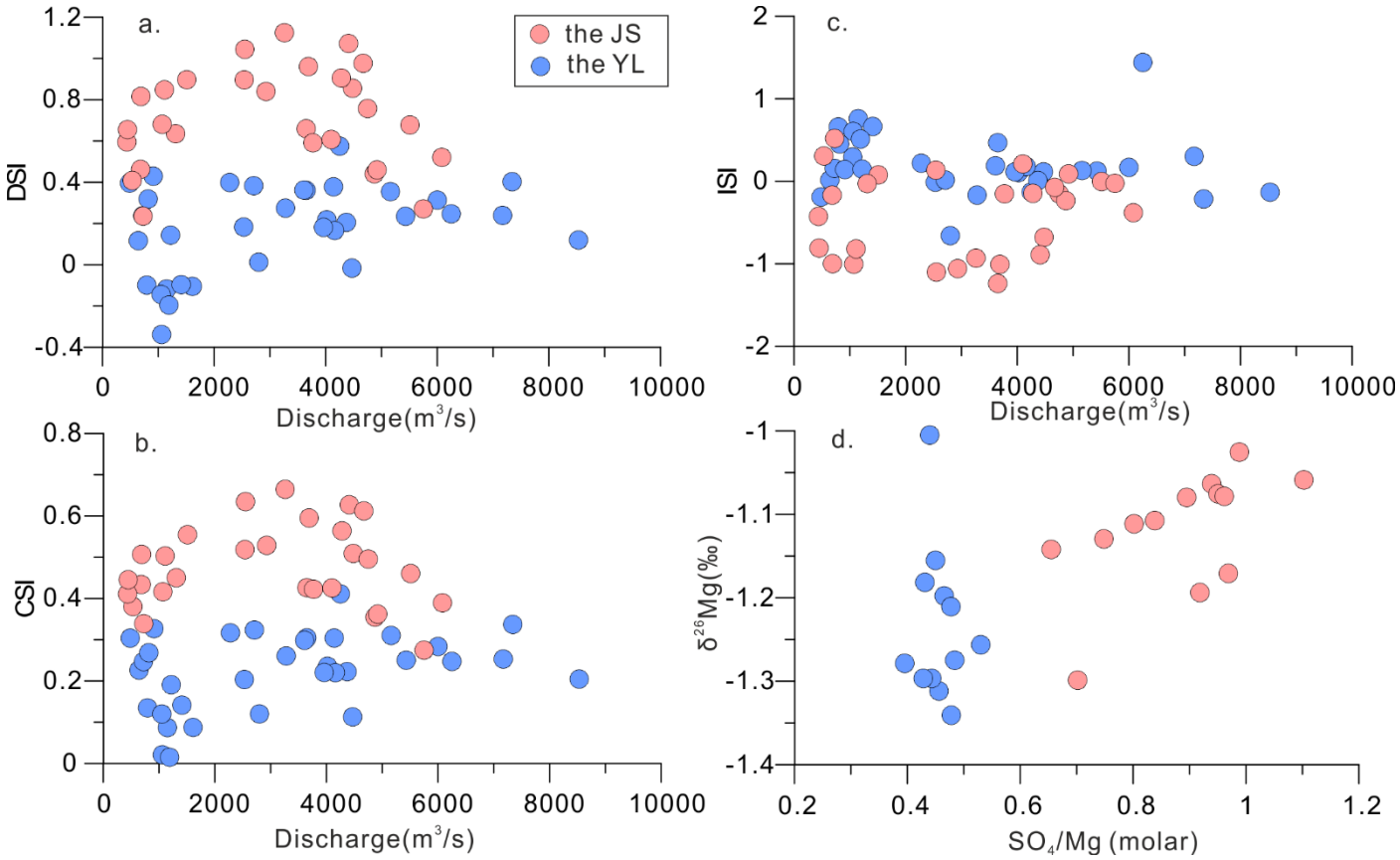

Fig. S4

References

Noh, H., Huh, Y., Qin, J., Ellis, A., 2009. Chemical weathering in the Three Rivers region of Eastern Tibet. Geochimica et Cosmochimica Acta 73, 1857-1877.